

ACTOPROBE LLC

ACTO-TERS



Table of Contents

1 INTRODUCTION	3
2 PROGRESS IN COMBINING ATOMIC FORCE MICROSCOPY WITH RAMAN SPECTROSCOPY FOR PIXEL SIDEWALLS CHARACTERIZATION	8
2.1 TERS Experiments	9
2.1.1 Dependence of TERS Enhancement on Gold Thickness	9
2.1.2 TERS on FPA Samples	12
2.1.3 Tip-enhanced stimulated Raman spectra on FPA samples	13
2.1.4 TERS with Tuning Fork Probes	14
2.1.5 STM probes	16
2.1.6 UHAR Tuning Fork and STM Probes	16
2.2 Near-field Scanning Optical Microscopy (NSOM)	17
3 FAR-FIELD RAMAN SPECTROSCOPY OF FPA SIDEWALLS	22
3.1 Introduction	22
3.2 Confocal Microscopy on FPA	22
3.3 Far-Field Raman Spectroscopy on FPA	24
3.3.1 Polarization Study	24
3.3.2 Comparison of Raman spectra from III-V and II- VI FPA materials	27
3.3.3 Raman from real SLS FPA structure	28
3.4 Conclusion	28
4 PROGRESS IN HIGH ASPECT RATIO AFM PROBE FABRICATION	30
4.1 High aspect ratio probes fabricated by Actoprobe	30
4.2 Probe testing with extended Z-piezo	31
4.3 AFM Scans on FPA Samples from SKinfrared and NVESD	33
4.3.1 SKinfrared sample	33
4.3.2 NVESD sample	36
5 FUTURE UPGRADES AND ACCESSORIES	39
5.1 AFM Active Optical Probe(AAOP)	39
5.2 Additional Raman lasers: UV, blue, green, infrared	39
5.3 Fast confocal scanning	40
5.4 Custom High NA objectives and Upright microscope configuration to increase Raman signal	43

5.5 Additional collection channel for NSOM imaging and Raman imaging at the same time	44
5.6 TERS probe development for improving consistency and enhancement	45
5.7 Polarization contrast	45
6 OPERATING PROCEDURES OF ACTOPROBE'S TERS SYSTEM	49
7 CONCLUSION	57

1 Introduction

Multicolor detector capabilities in the infrared are highly beneficial for various military and civil applications involving identification of temperature differences and determination of the thermal characteristics of an object. Among these applications are homeland security, industrial imaging, banks, facility security, custom control and law enforcement. Detectors based on interband (Mercury-Cadmium-Telluride, MCT) and intersubband (quantum well infrared detectors, QWIPs) transitions have been the dominant technologies for such applications. Difficulties in the epitaxial growth of MCT and low electron effective mass resulting in large dark current due to tunneling especially at longer wavelengths affect the development of multispectral cameras based on MCT. Compared to MCT detectors, QWIPs have a number of advantages, including the use of standard manufacturing techniques based on mature GaAs growth and processing technologies, highly uniform and well controlled MBE growth on larger area GaAs wafers, high yield and thus low cost, more thermal stability. However, they have larger dark currents and lower quantum efficiency compared to the interband devices.

On the contrary, the basic material properties of InAs/GaSb type-II strained layer superlattices (T2SL) provide a prospective benefit in the realization of dual-color imagers. The strain in the InAs/GaSb T2SL system facilitates suppression of interband tunneling²⁹ and Auger recombination.⁸ The larger effective mass in T2SL leads to a reduction of tunneling currents compared with MCT detectors of the same bandgap.²⁹ By optimizing the oscillator strength in this material system, a large quantum efficiency and responsivity can be obtained. Moreover, the commercial availability of substrates with good electro-optical homogeneity, and without large cluster defects, also offers advantages for T2SL technology. High performance InAs/GaSb T2SL detectors have been reported for the mid-wave infrared (MWIR), long-wave IR (LWIR), and very long wave IR (VLWIR) spectral regions. Moreover, mega-pixel FPAs, i.e. FPAs of sizes up to 1024x1024 have been demonstrated. Multiband T2SL structures were also realized, including short-wave IR(SW)/MWIR, MW/MWIR, MW/LWIR, LW/LWIR, and SW/MW/LWIR⁶ detectors and focal plane arrays (FPAs).

However, the performance parameters of T2SL detectors, in particular, the dark current densities, are still lower compared with the MCT benchmark. To realize T2SL-based focal plane arrays (FPAs) with high resolution the number of FPA pixels needs to increase with simultaneous scaling of the lateral dimensions of individual pixels. Then the FPA performance, with typical mesa dimensions of individual FPA pixels of 20umx20um, is strongly dependent on surface effects due to a large pixel surface/volume ratio. Thus, the development of the mesa delineation process followed by the appropriate passivation is crucial for the realization of high performance T2SL multicolor detectors.

To characterize the quality of etched sidewalls and conformal uniformity of the passivation layer, several techniques may be utilized, such as imaging by transmission electron microscopy (TEM) or scanning electron microscopy (SEM). While producing reliable results, both of these techniques require sample preparation, often destructive, to access the vertical etched or passivated surfaces of the detector. Thus, the device fabrication process is significantly slowed due to the impeded feedback on sidewall morphology after etching and passivation procedures.

Several variations of the AFM technique have been developed for vertical sidewall profiling of micro- and nanostructures. These AFM-based methods can probe the surface defects on close to vertical surfaces with good accuracy, however, they are unable to characterize the chemical composition of the defects. In this report we present a technique based on confocal Raman spectroscopy combined with high resolution AFM that enables non-destructive characterization of sidewall profiles as well as chemical composition of etched and passivated small (24umx24um) focal plane array (FPA) features

ACTOPROBE LLC

801 University S.E., Suite 100, Albuquerque, New Mexico, 87106

Phone: +1 (505) 272-7176; Email: aukhanov@actoprobe.com;

www.actoprobe.com

fabricated from LW/LWIR InAs/GaSb type-II strained layer superlattice (T2SL) detector material. Furthermore, the combination of Atomic Force Microscope with Tip-Enhanced Raman Spectroscopy (AFM/TERS) is discussed. These techniques will be of great advantage for efficient T2SL FPA development.

The overall objective of this Phase II SBIR project was **to demonstrate the feasibility of Actoprobe's instrument** (see Fig. 1.1.), a combined Atomic Force Microscope/Tip-Enhanced Raman Spectroscopy (AFM/TERS) for non-destructive characterization of detector side-wall morphology, electrical and chemistry characteristics. The successful development of this instrument will satisfy the market demand for efficient FPA pixel-sidewall characterization and assist in optimizing passivation techniques for MCT and SLS detectors. It supports the US Army strategic goal to develop more efficient and effective night vision equipment. This Final Report summarizes the progress for all tasks performed under the Phase II effort.

During the project, we completed four basic activities: we A) Combined Atomic Force Microscopy (AFM) and Tip Enhanced Raman Spectroscopy (TERS) (Fig. 1.1) for non-destructive characterization of detector pixel side-wall as for morphology, as well as electrical and chemical characteristics; B) Tested various modes of the AFM system, including tapping mode (Fig. 1.2a), tuning fork (Fig. 1.2b) and scanning tunneling microscopy (STM) probes (Fig. 1.2c), for better enhancement of the Raman signals and developed different configurations, upright (Fig. 1.3, 1.4 and 1.6) and oblique (Fig. 1.3~1.5), for laser excitation and raman signal collection and; C) Developed and fabricated high aspect ratio AFM optical probes (Fig. 1.7) for characterization of detector pixel side-walls with angles up to 80 degrees and depths up to 10 μm , and demonstrated stimulated Raman signals; and D) designed the AFM Active Optical Probe and its fabrication process. These three activities (A-D) supported the SBIR Phase II goal to successfully develop an instrument for the infrared detector industry to characterize FPAs, optimize passivation techniques for these devices and ultimately improve their performance at low light condition.

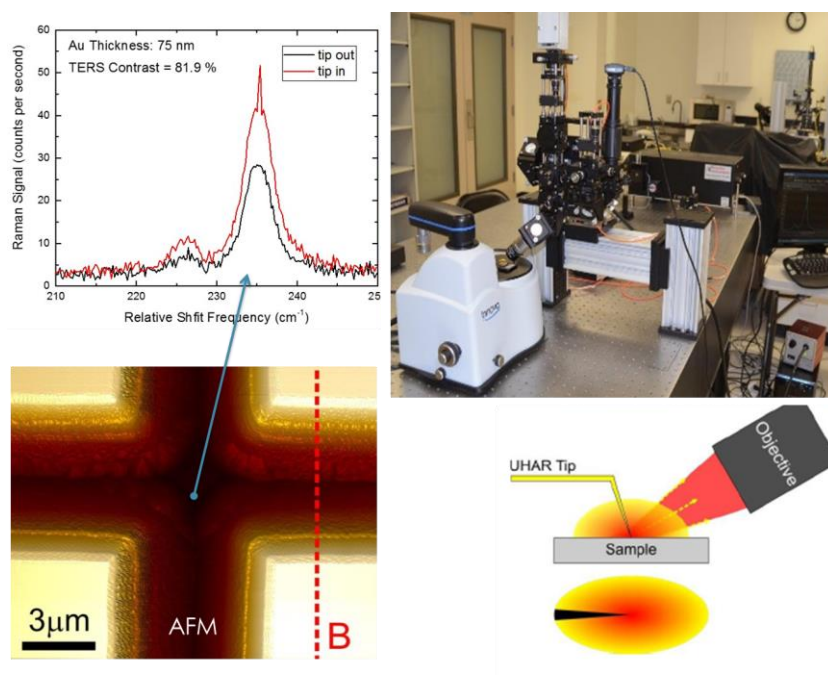


Figure 1.1 Actoprobe's TERS instrument combining AFM, confocal microscope and spectrometer

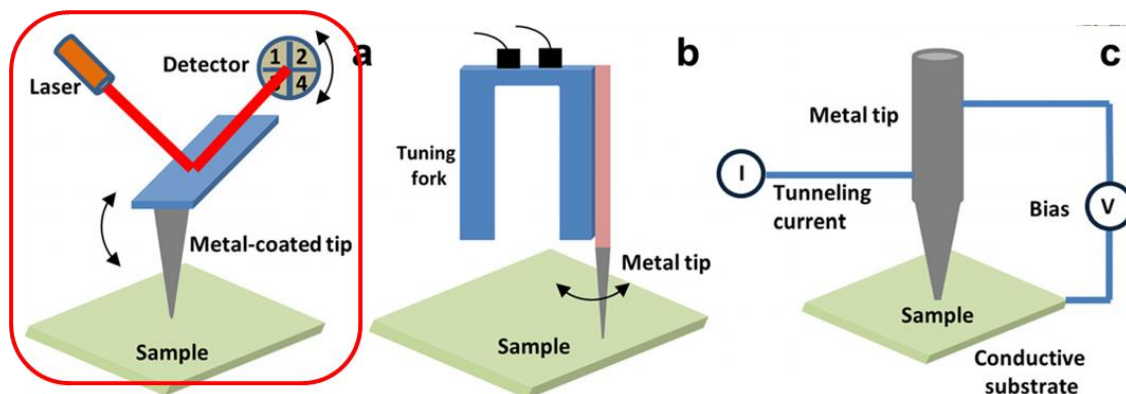


Figure 1.2 AFM modes for TERS setup (a) tapping mode (b) tuning fork (c) STM

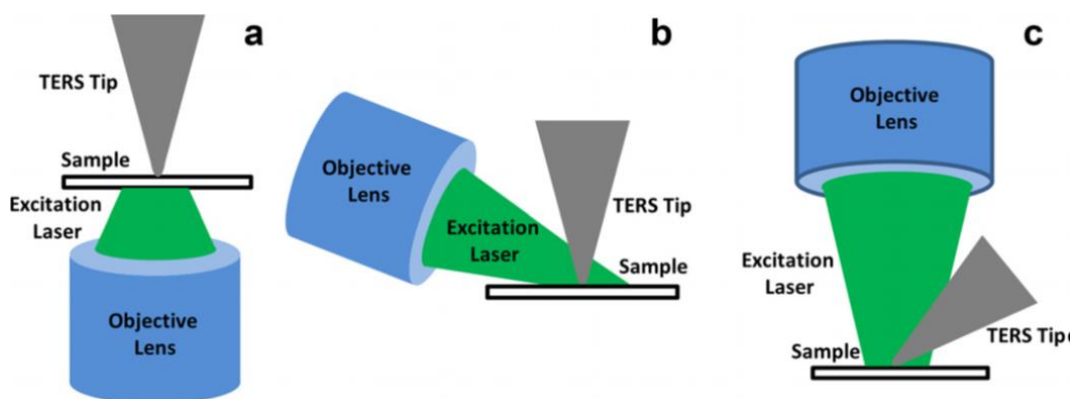


Figure 1.3 Excitation configurations for TERS setup (a) backside (b) oblique (c) upright

Upright and Oblique TERS Setup

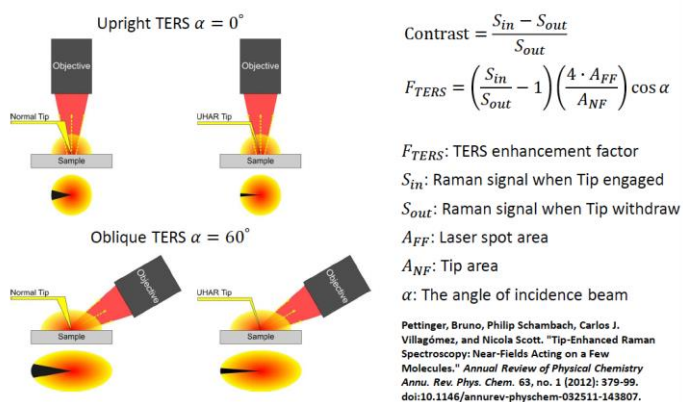


Figure 1.4 Comparison between upright and oblique TERS setup

Figure 1.5 Oblique configuration of Actoprobe's TERS system

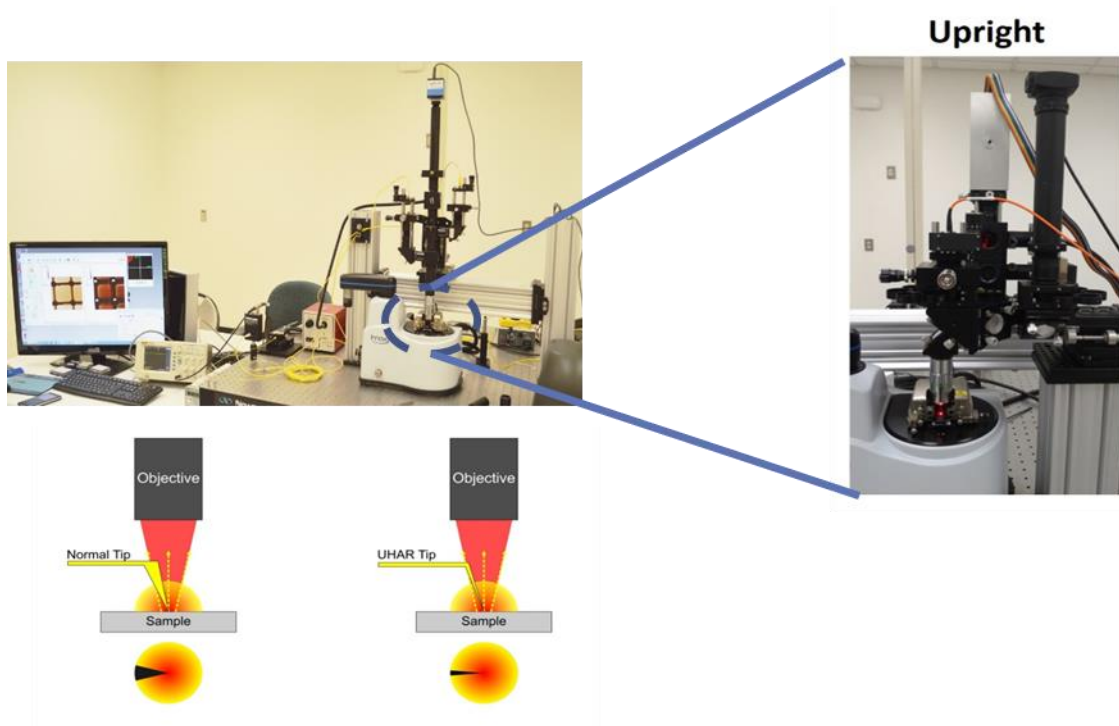


Figure 1.6 Upright configuration of Actoprobe's TERS system

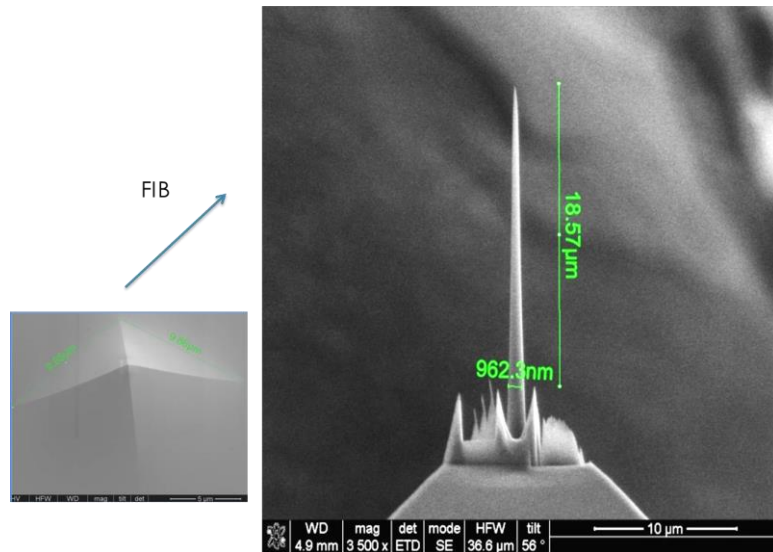


Figure 1.7 New High Aspect Ratio AFM probes had been developed for NVESD

2 Progress in combining Atomic Force Microscopy with Raman spectroscopy for pixel sidewalls characterization

2.1.2 TERS on FPA Samples

Figure 2.6 compare the TERS spectra on the top and the bottom of the FPA sample using an UHAR tapping mode probe. The Raman signal is significantly enhanced for the TO phonon. The TO and LO spectra vary along the sidewall due to material composition change and optical polarization relative to the surface, as shown in Fig. 2.7. The spectra change along the sidewall also confirms the nanometer scale near-field resolution of Actoprobe's TERS system.

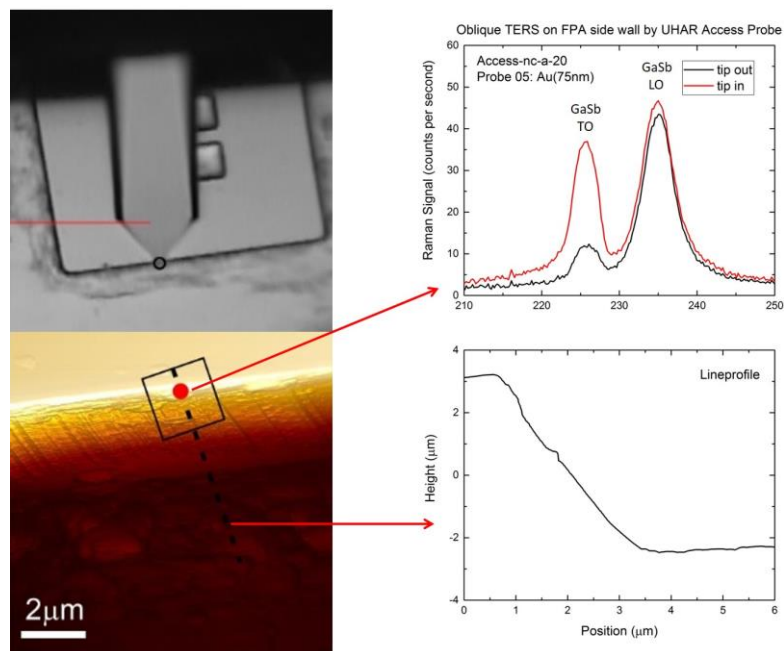


Figure 2.6 Oblique TERS Experiments on FPA samples

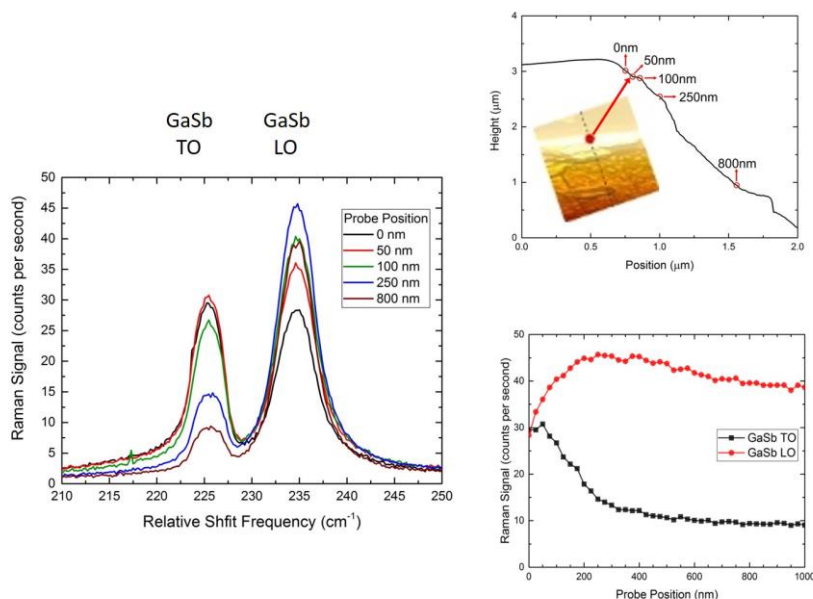
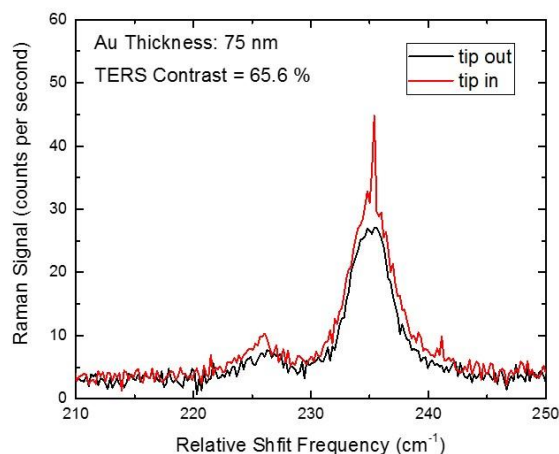
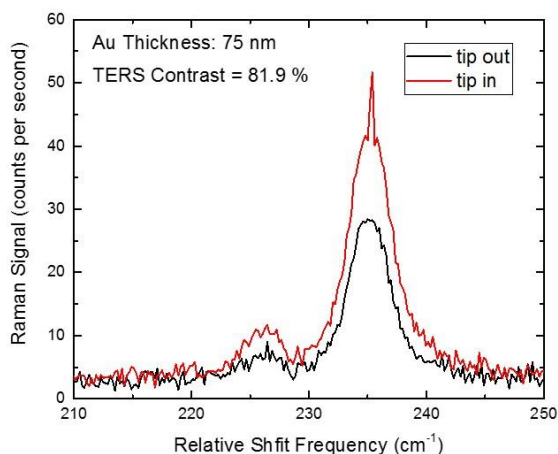


Figure 2.7 Comparison of TERS spectrum along the sidewall

2.1.3 Tip-enhanced stimulated Raman spectra on FPA samples

Figure 2.8 shows the evidence of stimulated Raman scattering with TERS through the AFM tip at two different position along FPA side wall. Tapping mode HAR probe with gold coating of 75nm is used. Contrast as high as 82% is achieved with the tip-enhanced stimulated Raman spectrum. Fig. 2.9 shows the measurement on the screen for the spectrometer.

Evidence of Stimulated Raman Scattering



Probe #05 – Au (75nm)

Probe #06 – Au (75nm)

Figure 2.8 Evidence of stimulated Raman scattering at two different positions along the side wall

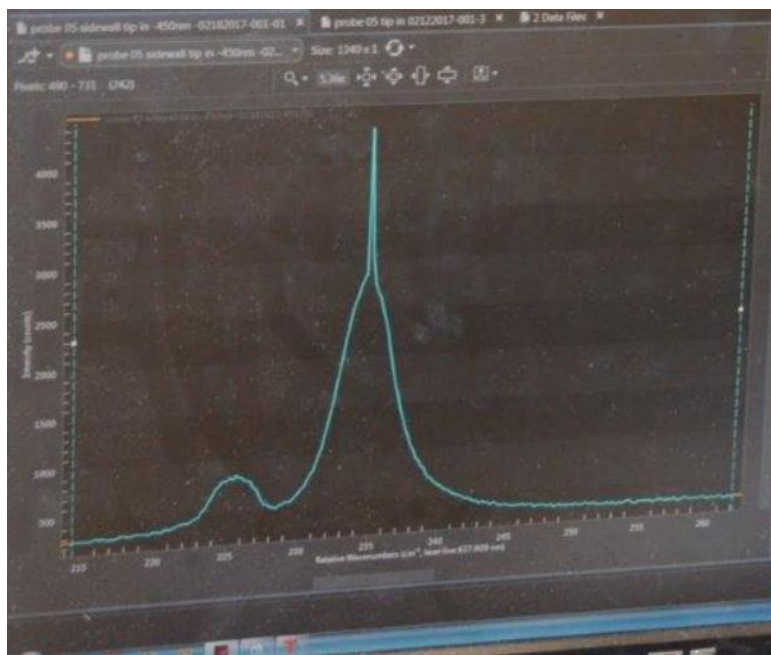


Figure 2.9 Evidence of stimulated Raman scattering on the spectrometer screen

2.1.4 TERS with Tuning Fork Probes

The schematic and the SEM image of Actoprobe's tuning fork probes are shown in Fig. 2.10. Unlike tapping mode probes which are made of silicon and coated with gold, tuning fork probes are made out of very thin gold wires. As a result, it is easy to achieve a TERS contrast of more than 100% with tuning fork probes because of stronger surface plasmon excitation. An example of TERS on Si with tuning fork probe is illustrated in Fig. 2.11. For FPAs, the TERS experiment is done at the bottom (Fig. 2.12) and in the middle (Fig. 2.13) of the FPA sidewall. When the tip is at the bottom a contrast of 133% is achieved for the LO but only 78% for the TO spectrum. On the contrary, when the tip is in the middle of the sidewall, the TO spectrum shows an 184% enhancement while the LO only 50%.

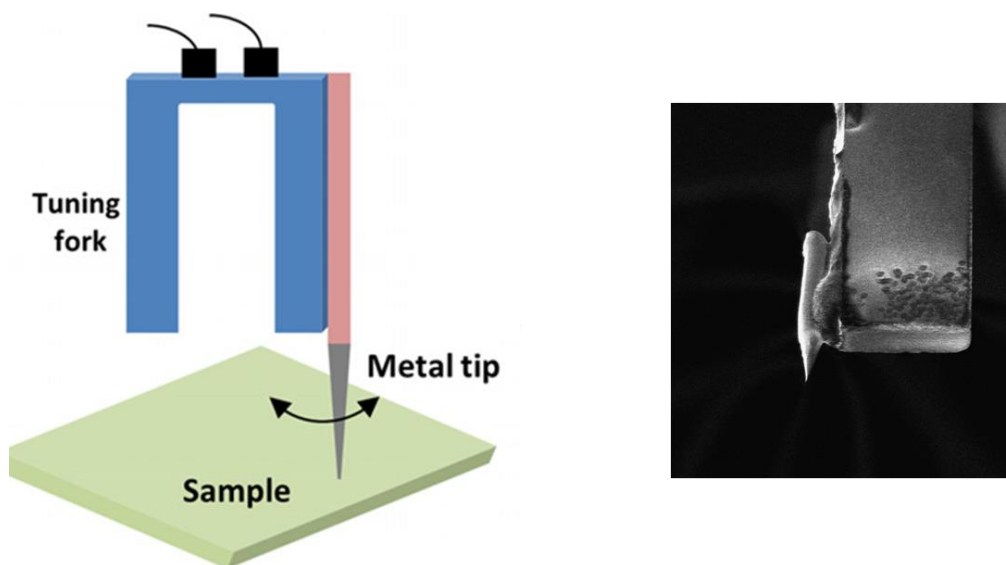


Figure 2.10 Schematic (left) and SEM image (right) of Actoprobe's tuning fork probes

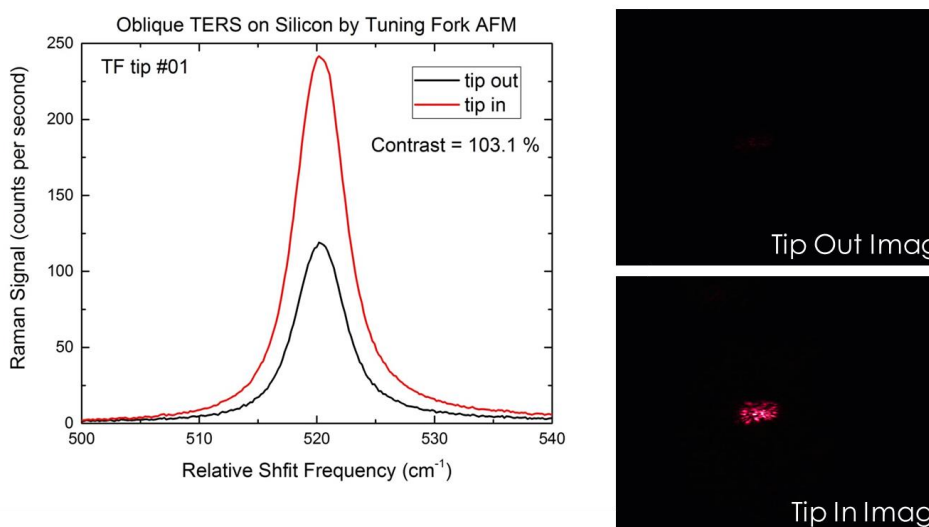


Figure 2.11 TERS on Si by tuning fork probes

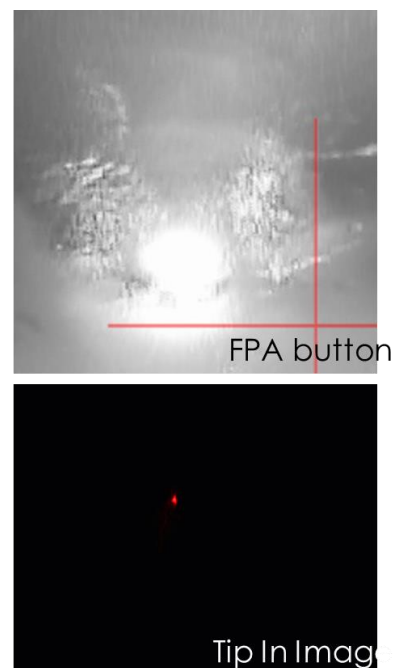
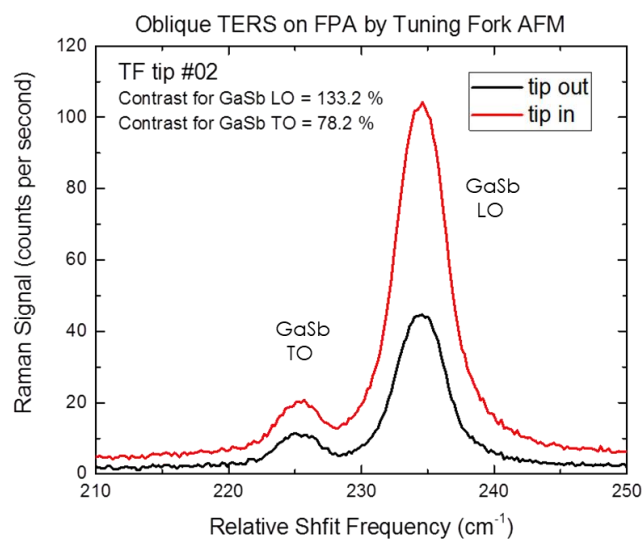


Figure 2.12 TERS on the bottom FPA by TF probes

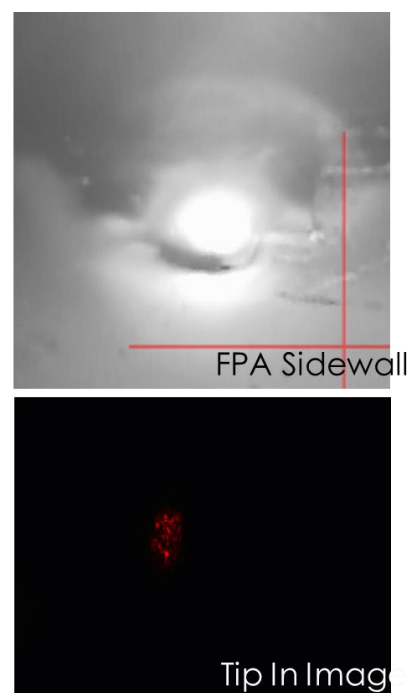
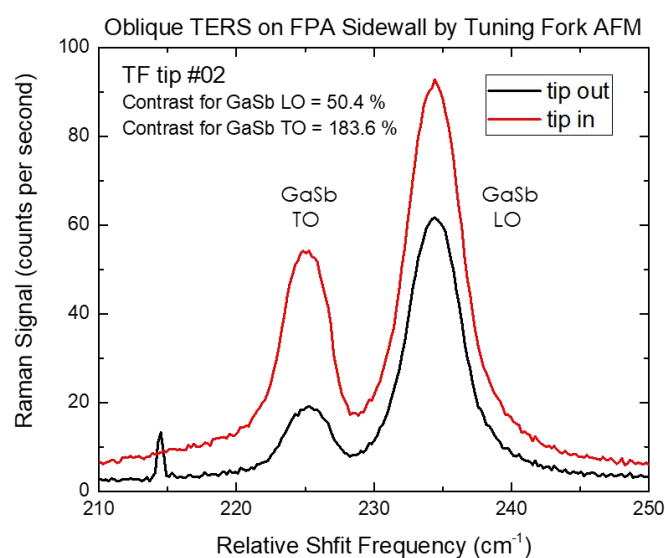


Figure 2.13 TERS on FPA sidewall by TF probes

2.1.5 STM probes

Like tuning for probes, the STM probes are made of very thin gold wires and should have stronger surface plasmon excitation than tapping mode probes. However, to use STM mode of the AFM system, the surface of the sample needs to be conductive, and for an FPA sample requires more sample preparation (i.e. removal of passivation and/or oxide). Hence the TERS experiment with STM probes will be done in future research.

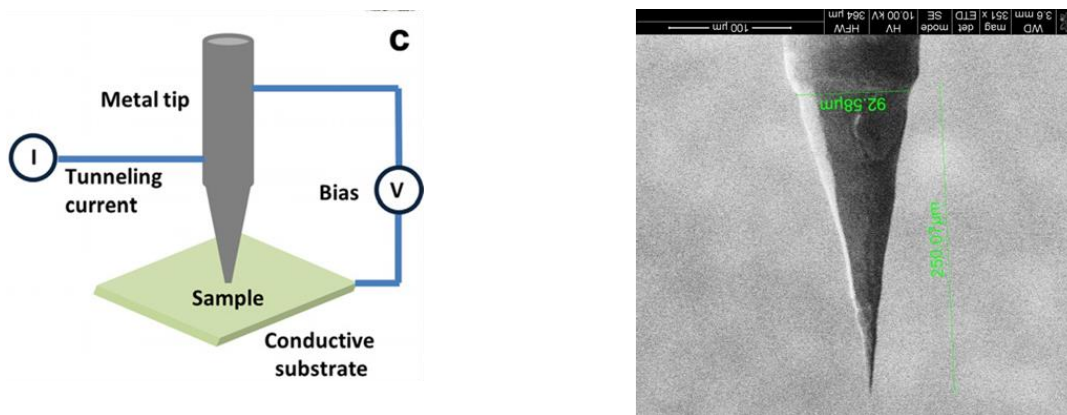


Figure 2.14 Schematic (left) and SEM image (right) of Actoprobe's STM probes

2.1.6 UHAR Tuning Fork and STM Probes

Tuning fork and STM probes can also be milled to have very high-aspect ratio as in UHAR tapping mode probes for deep trench characterization of FPAs. Fig. 2.15 and Fig. 2.16 show the examples of UHAR tuning fork and STM probes, respectively, made by Actoprobe. TERS experiment will be conducted when the optimal probe geometry is determined in future research.

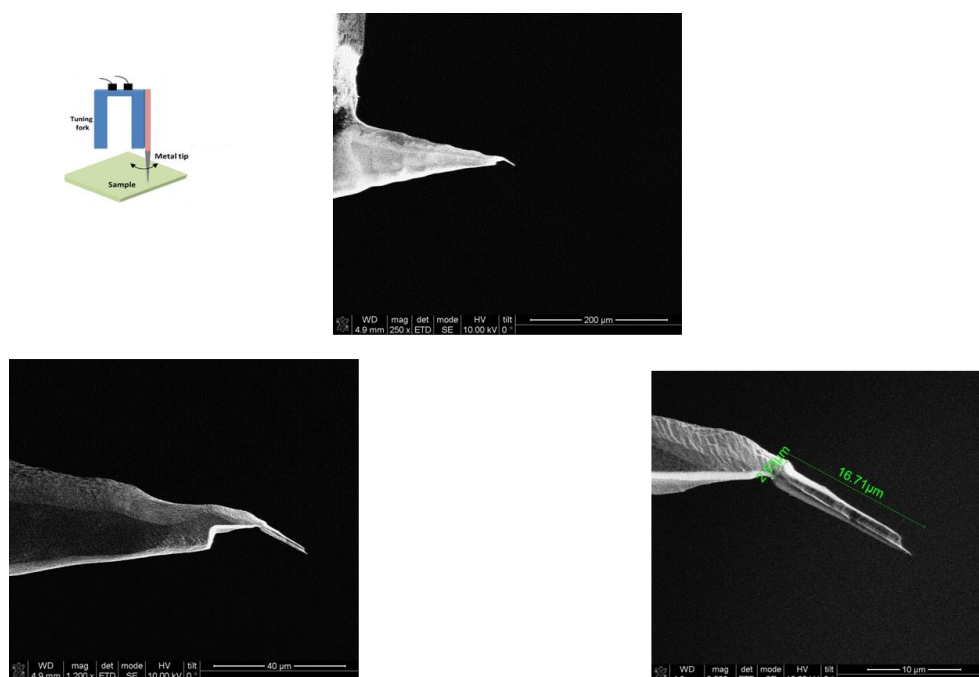


Figure 2.15 An example of Actoprobe's UHAR Tuning Fork probes

ACTOPROBE LLC
801 University S.E., Suite 100, Albuquerque, New Mexico, 87106
Phone: +1 (505) 272-7176; Email: aukhanov@actoprobe.com;
www.actoprobe.com

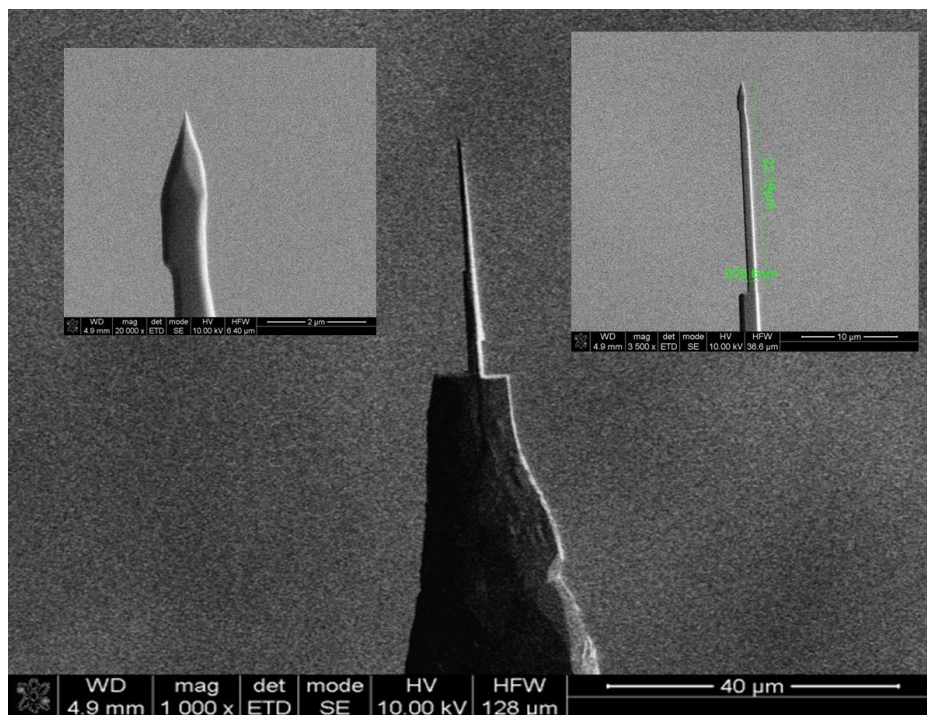


Figure 2.16 An example of Actoprobe's UHAR STM probes

2.2 Near-field Scanning Optical Microscopy (NSOM)

Actoprobe's TERS system can also be used for NSOM experiment as shown in Fig. 2.17 with a red laser excitation (637nm). The AFM image shows the conventional AFM scan of the FPA sample and the corresponding NSOM image is taken at the same time as AFM scan. Because tip apex and surface produce laser cavity effect, interference fringes appear on the sidewalls. The fringe widths depend on the wavelength of the laser (see Fig. 2.18 for IR laser at 1310nm and Fig. 2.19 for green laser at 532nm) and the refractive index of the material. As a result, the thicknesses of different layers can be derived by analyzing the fringe patterns of the NSOM scan. Fig. 2.20 shows the calculation of fringe ratio between different wavelengths for the two materials GaSb and InAs, and the result is plotted in Fig. 2.24. The experimental data of the fringe ratio can be calculated using the detailed plot shown in Fig. 2.21 to Fig. 2.3 and is plotted in Fig. 2.24. Since the material consists of the two materials, the ratio from the experimental data falls in between the ratio of GaSb and that of InAs, and its values is a linear combination of the two. Therefore, the composition of the SLS structure can be derived to be consisted of ~ 5ML of GaSb and 7- 6 ML of InAs. Or at least we expect that the ratio of thickness is SLS structure GaSb to InAs should be ~ 5/6.5, i.e. more more InAs than GaSb.

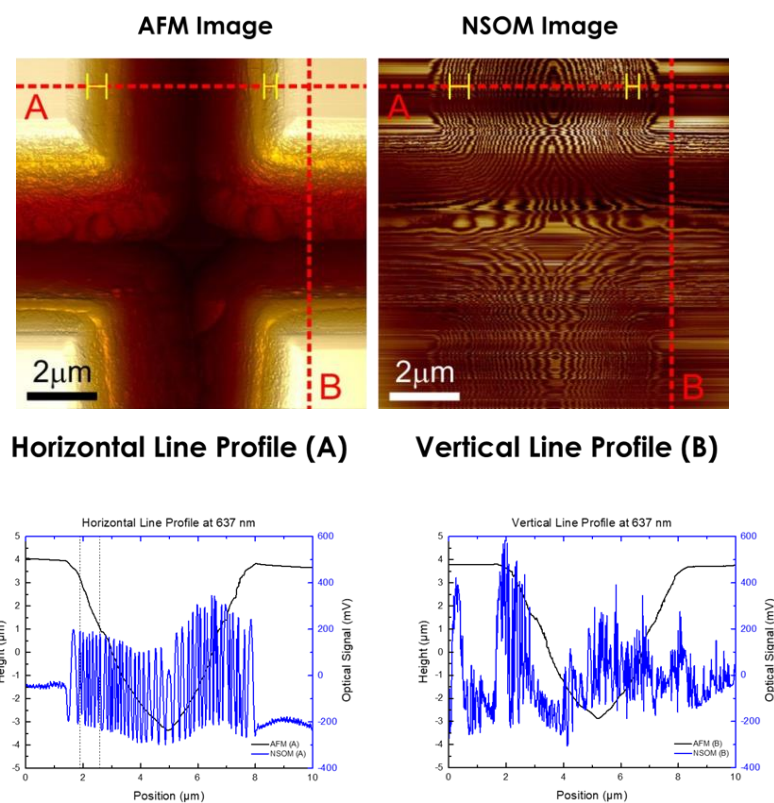


Figure 2.17 AFM and NSOM image Line Profiles by Red Laser (637 nm)

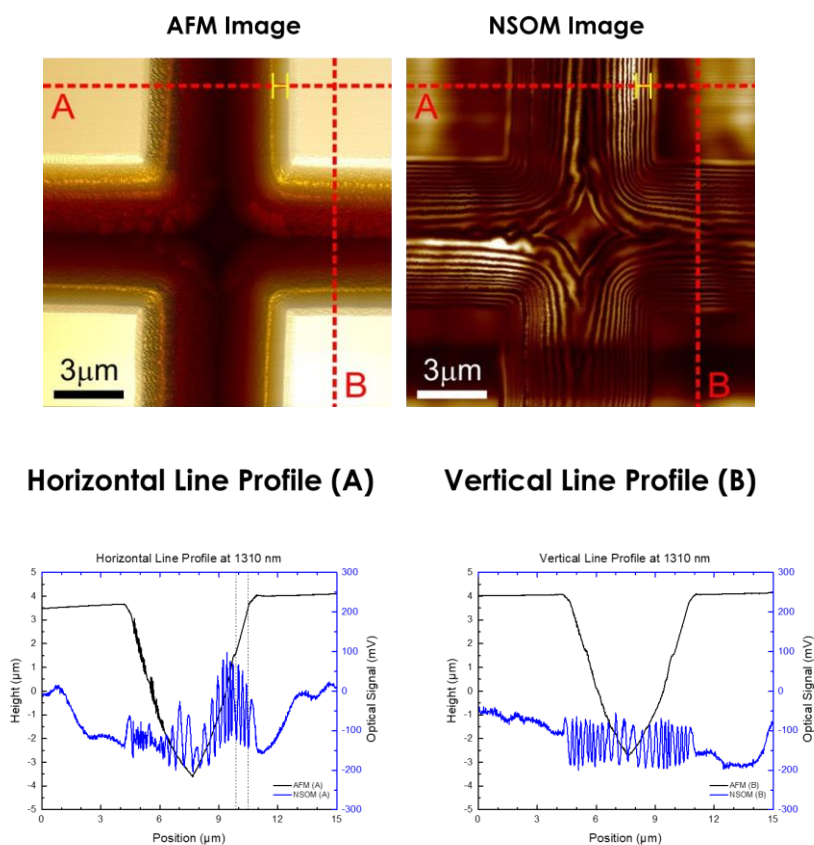


Figure 2.18 AFM and NSOM image Line Profiles by IR Laser (1310 nm)

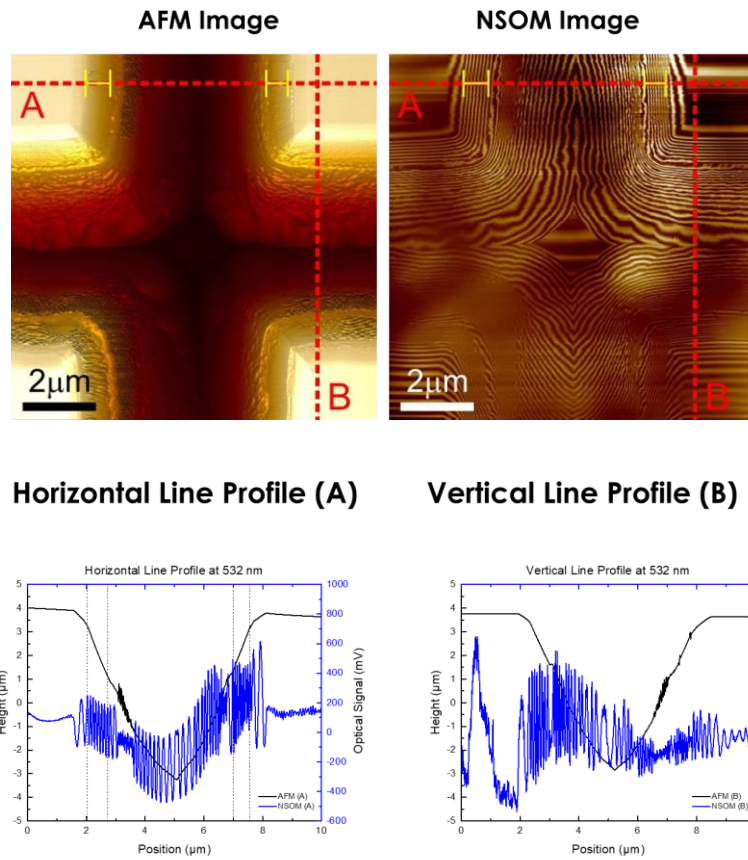


Figure 2.19 AFM and NSOM image Line Profiles by Green Laser (532 nm)

	Wavelength (nm)	Refractive Index		Fringe Width (nm)	Refractive Index Ratio : Experiment
		GaSb	InAs		
Ratio 1 Green To Red	$\lambda_G = 532$	$n_G = 4.4986$	$n'_G = 4.3736$	$W_G = 96.4$	
	$\lambda_R = 637$	$n_R = 5.1409$	$n'_R = 3.9547$	$W_R = 115.5$	
	$\lambda_R/\lambda_G = 1.20$	$n_R/n_G = 1.14$	$n'_R/n'_G = 0.90$	$W_R/W_G = 1.20$	
Ratio 2 Green To NIR	$\lambda_G = 532$	$n_G = 4.4986$	$n'_G = 4.3736$	$W_G = 71.6$	
	$\lambda_{NIR} = 1310$	$n_{NIR} = 4.1292$	$n'_{NIR} = 3.532$	$W_{NIR} = 205.1$	
	$\lambda_{NIR}/\lambda_G = 2.68$	$n_{NIR}/n_G = 0.92$	$n'_{NIR}/n'_G = 0.81$	$W_{NIR}/W_G = 2.86$	
Ratio 3 Red To NIR	$\lambda_R = 637$	$n_R = 5.1409$	$n'_R = 3.9547$	$W_R = 115.5$	
	$\lambda_{NIR} = 1310$	$n_{NIR} = 4.1292$	$n'_{NIR} = 3.532$	$W_{NIR} = 268$	
	$\lambda_{NIR}/\lambda_R = 2.06$	$n_{NIR}/n_R = 0.80$	$n'_{NIR}/n'_R = 0.89$	$W_{NIR}/W_R = 2.32$	

$$\text{Assume } W \propto \frac{\lambda}{n}; \quad \frac{n_2}{n_1} = \frac{W_1}{W_2} \cdot \frac{\lambda_2}{\lambda_1}$$

Figure 2.20 Fringes ratio calculation

Wavelength = 532 nm

Wavelength = 637 nm

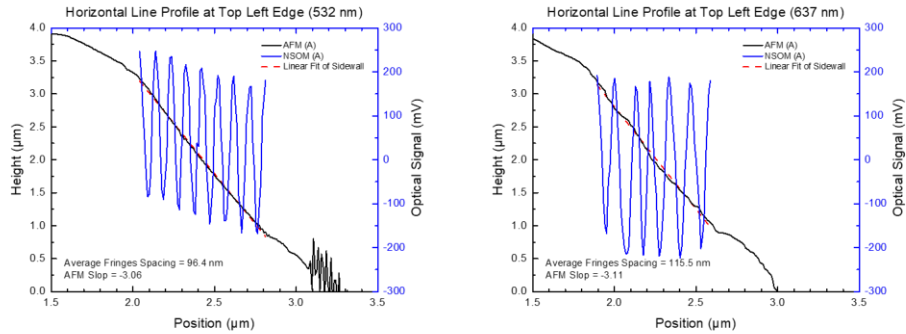


Figure 2.21 AFM and NSOM Horizontal Line Profile at Top Left Edge

Wavelength = 532 nm

Wavelength = 1310 nm

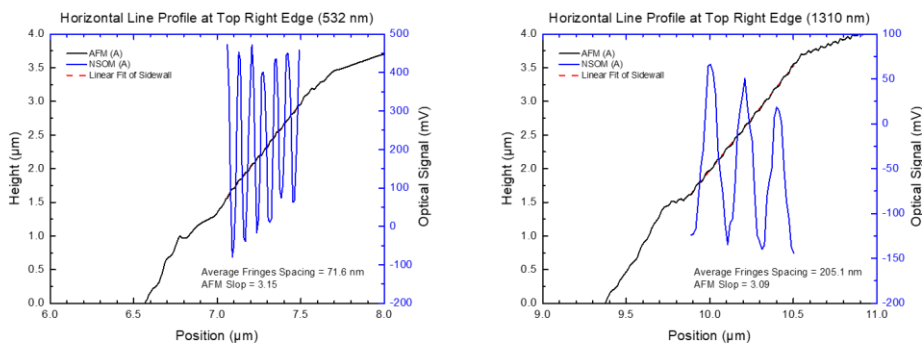


Figure 2.22 AFM and NSOM horizontal line profile at top right edge

Wavelength = 637 nm

Wavelength = 1310 nm

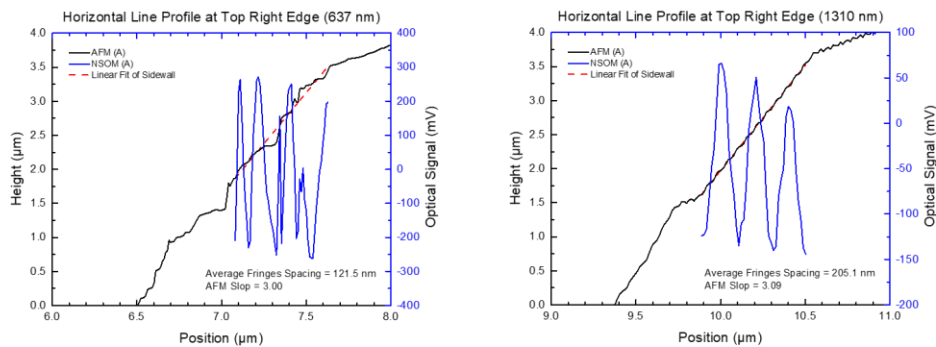


Figure 2.23 AFM and NSOM horizontal line profile at top tight edge

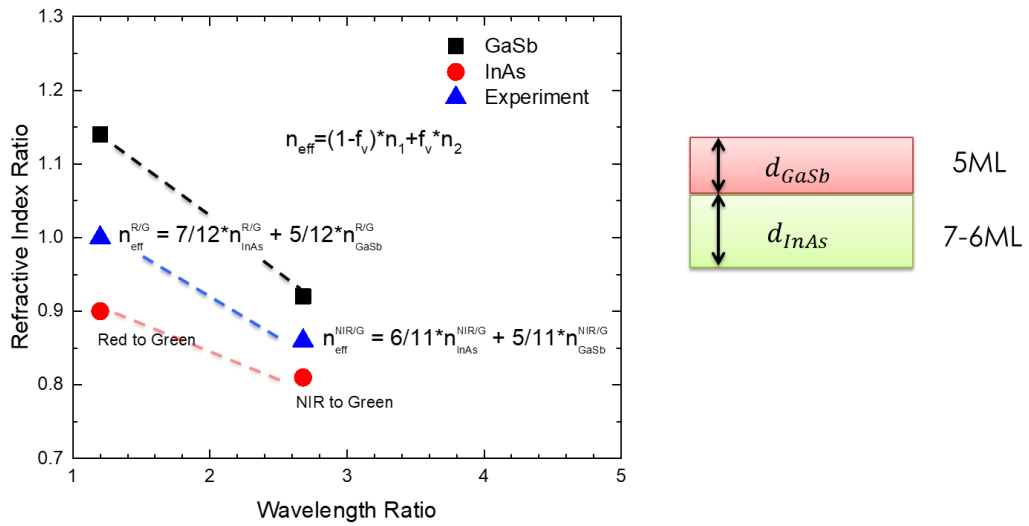


Figure 2.24 Thickness analysis of GaSb and InAs

3 Far-Field Raman spectroscopy of FPA sidewalls

3.1 Introduction

For the design of a combined Raman AFM instrument, it is important to investigate a FPA with conventional Raman spectroscopy in order to gain a better understanding of issues and challenges involved in such a study. It should also help to choose an appropriate spectrometer and laser source for the future instrument. Furthermore, in far-field, we could use diffraction-limited microscope objective with a dry numerical aperture of 0.95 and up to 1.3 in immersion oil. As a result, the laser can be focused four to ten times smaller as compared to the TERS setup.

3.2 Confocal Microscopy on FPA

We performed confocal imaging experiments on FPA samples with 6.7 μm deep trenches. The experimental set up is the Actoprobe Acto S confocal microscope, presented in Figure 1.1. The FPA was mounted on the AFM X-Y scanner (we used a CP research $100 \times 100 \mu\text{m}$ piezo scanner) and scanned in raster-scan fashion. We scanned the FPA from top to bottom of the pixel in 250 nm slices using $18 \times 18 \mu\text{m}$ range with $100 \times 0.9\text{NA}$ objective: First we took a slice on the top of the pixel, then moved the objective (focal point) by 250 nm and repeated (we used the Z piezo to move the objective). We took all together 33 slices (optical sectioning). We used single mode fiber of 3 μm mode field diameter (i.e. the confocal aperture size was 3 μm) with 405 nm blue laser to illuminate the sample. The data was collected through ultra-sensitive femto-watt silicon detector. The data is presented in Figure 3.1.

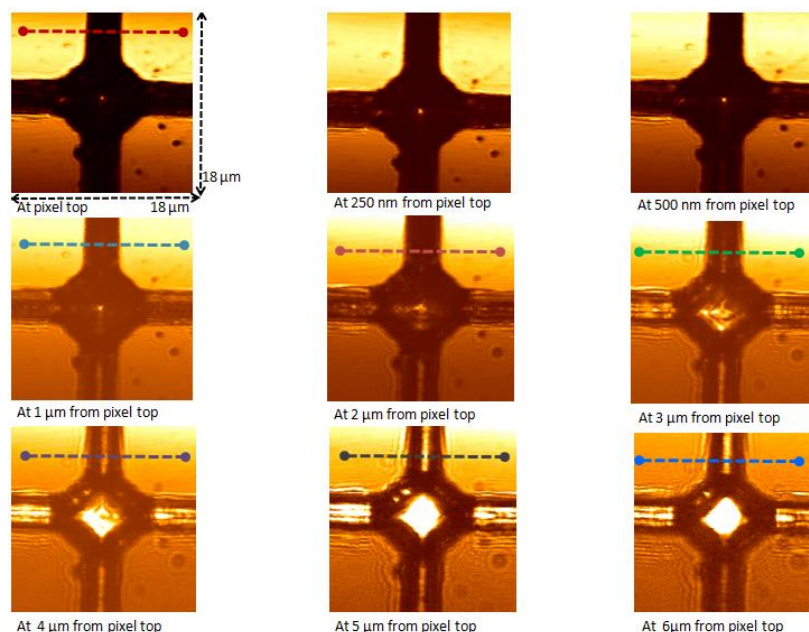


Figure 3.1 Confocal images of FPA with 6.7 μm deep trenches. The image size is $18 \times 18 \mu\text{m}$. Images are taken at different depths from the pixel top. The dashed lines (different colors) inside the figures correspond to the cross sections used to create the FPA side wall profile in Fig. 3.2. The data suggests the resolution to be better than 50nm lateral and 150nm Z.

Each scan size was $18 \times 18 \mu\text{m}$. We achieved lateral resolution of $\sim 50\text{nm}$ and Z resolution of $\sim 150\text{nm}$ using a $100\times$ objective with 0.9NA at 405 nm wavelength. As we move toward the bottom, the features on the top of the pixel get out of focus while the features that were below (on the pixel walls in this case) start showing up with each slice. No two slices are identical; optical sectioning achieved through confocal imaging is a very powerful tool, providing differentiation (among different planes) based on real features (on particular planes (slices)). This way we can tell the location of certain features at different planes, hence achieving full morphology (Figure 3.2). The images presented here show results of a proof of feasibility study. Higher resolution for Phase II can be achieved using smaller aperture size, an objective with higher NA and a lens pair with higher NA).

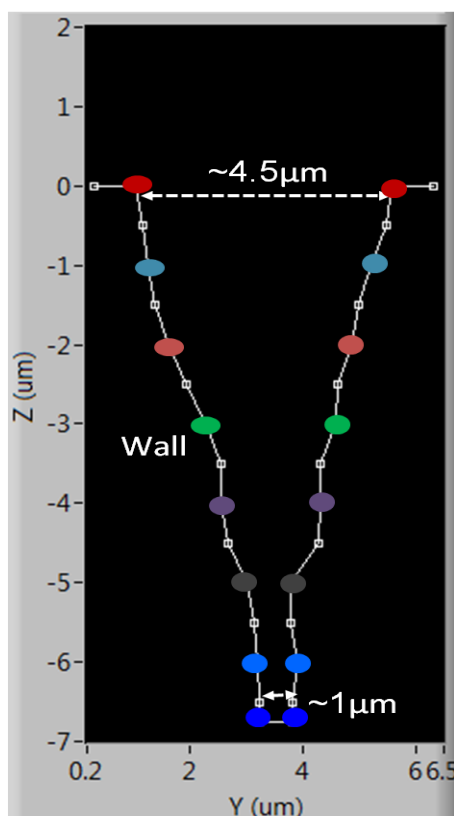


Figure 3.2 FPA side wall profile achieved through optical sectioning. The different color data points are extracted from the cross sections in Figure 3.1.

Figure 3.2 shows a FPA side wall profile extracted from line cross sections of different slices. Through the proposed setup, we expect to obtain real side wall profiles much better than what was presented in Figure 3.1. Confocal imaging techniques will provide high resolution optical images (with spectral information) which can be used to extract the real features at places where AFM tip cannot reach.

3.3 Far-Field Raman Spectroscopy on FPA

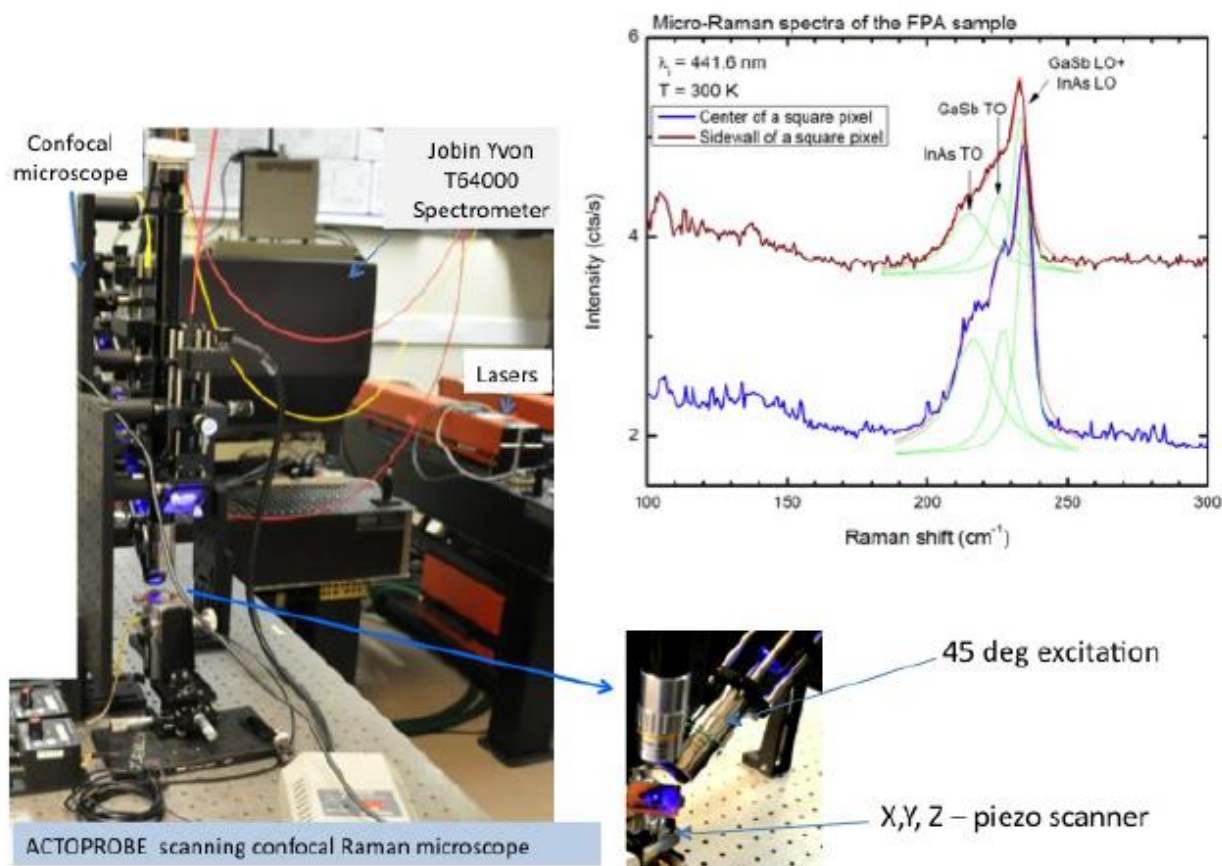


Figure 3.3 Experimental setup for confocal Raman spectroscopy.

We applied a Confocal Raman Microscope (ACTO-S, Actoprobe LLC product) combined with Jobin Yvon T64000 triple spectrometer (resolution 0.1cm^{-1}), and equipped with a liquid nitrogen cooled multichannel CCD (Fig. 3.3). A 441.6nm line of a He-Cd laser (100mW) was used for Raman excitation. The experimental setup is shown in Figure 15. A 45° excitation is applied to reduce elastically scattered laser light collected by the objective as shown in the figure. Also, the laser polarizations of incident and scattered light can be controlled using polarization rotators and filters to effectively measure Raman scattering on transverse optical phonons (TO, corresponding to atoms oscillating perpendicular to phonon propagation) and longitudinal phonons (LO, corresponding to oscillations along phonon propagation), according to Raman selection rules.

3.3.1 Polarization Study

Micro-Raman spectra of the $24\text{um} \times 24\text{um}$ mesa of T2SL FPA with $6:7\text{um}$ etch depth are shown in Figure 3.4. The spectra were measured at different points of the sample: the center of the mesa (1), two points on the sidewall (2,3), the center of the etched trench (4), and the crossing of the trenches (5). Spectrum 1 corresponds to the unetched SL, the strongest features are associated with the LO phonons of InAs at $\sim 237\text{cm}^{-1}$. This is in agreement with the Raman selection rules: in crystals of zinc blende structure only LO phonons are allowed in backscattering from the (001) surface.⁴ GaSb LO phonons are weaker and broader due to the smaller thickness of GaSb layers in the SLs. (The SL thickness is much

larger than the penetration depth of the laser light, therefore the substrate signal is suppressed in the spectra from the unetched region.) In contrast, spectrum 5 (from the deepest etched area) is dominated by the LO phonons of GaSb, associated with the GaSb substrate. InAs phonons are still present at lower intensity, which is probably due to the contribution of nearby sidewall regions. The spectra from the sidewall regions (2-4) show equally strong features of InAs LO and TO phonons. This is due to the deviation from backscattering geometry along the (001) direction. GaSb TO phonon features are also present, their intensity increases as the laser spot moves closer to the center of the etched trench (spectrum 4). This behavior can be explained by the increased contribution of the GaSb substrate or buffer layer in the deeper etched regions. Peaks associated with InAs phonons in the sidewall spectra are significantly broader compared to the unetched pixel top. This is due to structural disorder (poorer crystalline quality) on the sidewalls resulting from etching damage.

It is important to point out here that the Raman data presented in Figure 3.4 is obtained under normal laser excitation in contrast to Fig. 3.5, where laser excitation was applied at 45 degree with respect to the sample surface in order to reduce elastically scattered laser light collected by the objective. With the laser excitation at 45 degree, the polarizations of incident and scattered light can be independently controlled using polarization rotators and filters to effectively measure Raman scattering on transverse optical phonons (TO, corresponding to atoms oscillating perpendicular to phonon propagation) and longitudinal phonons (LO, corresponding to oscillations along phonon propagation), according to the Raman selection rules. Analysis of the Raman spectra demonstrated that TO phonon peaks can be utilized for characterization of the pixel sidewall quality. Raman peaks corresponding to both InAs and GaSb phonons carry information about material quality on the pixel sidewalls. This information is contained in both peak intensity and width. We can see that the peak width (FWHM) is increased (by 1.24cm⁻¹ and 1.68cm⁻¹ for InAs and GaSb phonons, respectively) at the sidewalls compared to the pixel top, likely due to defects introduced by the plasma etching process. Since both peak magnitude and width are affected, the phonon intensity is characterized by the area under the Raman peak (integrated intensity). The integrated intensity of the InAs peak is observed to decrease by 42% for InAs and 30% for GaSb on sidewalls, compared to the pixel top. This might suggest that InAs is more severely affected by the plasma etch than GaSb.

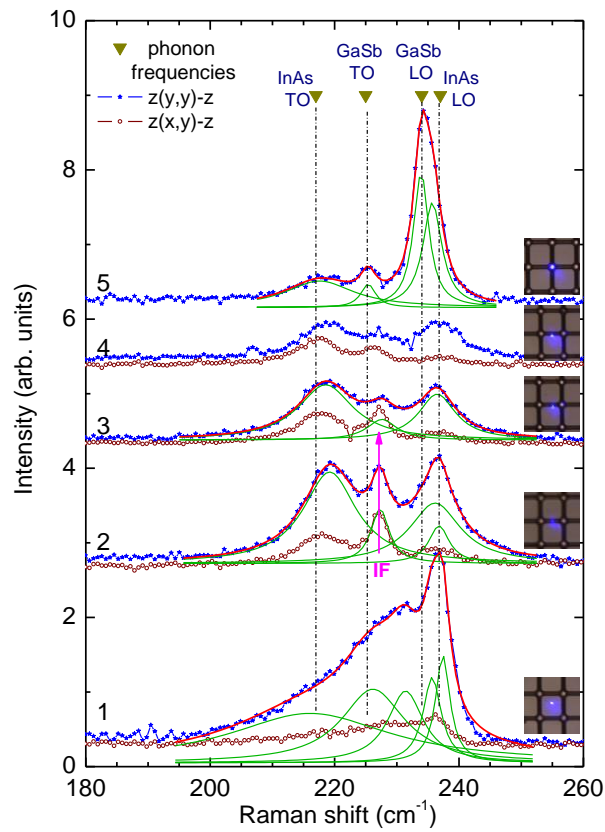


Figure 3.4 Transition of the Raman spectrum from the bottom to the top of the sidewall in upright configuration

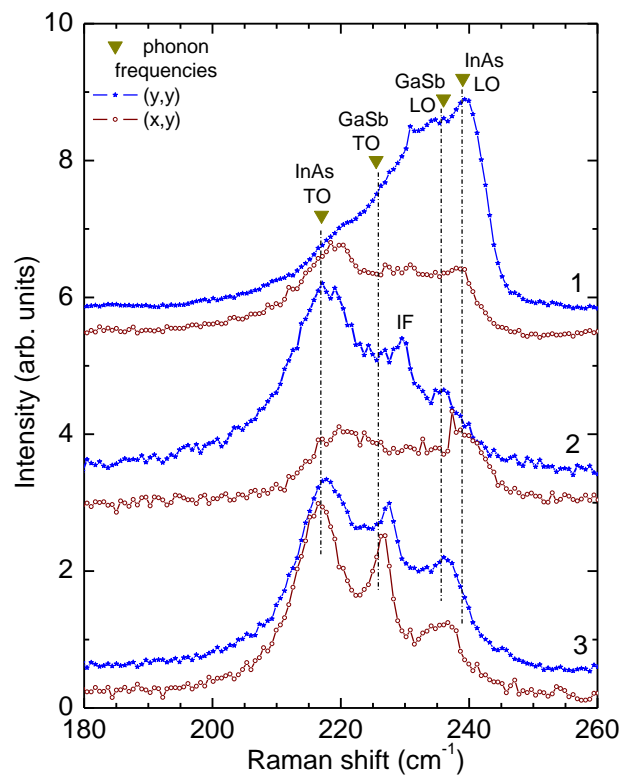


Figure 3.5 Transition of the Raman spectrum from the bottom to the top of the sidewall in oblique configuration

3.3.2 Comparison of Raman spectra from III-V and II- VI FPA materials

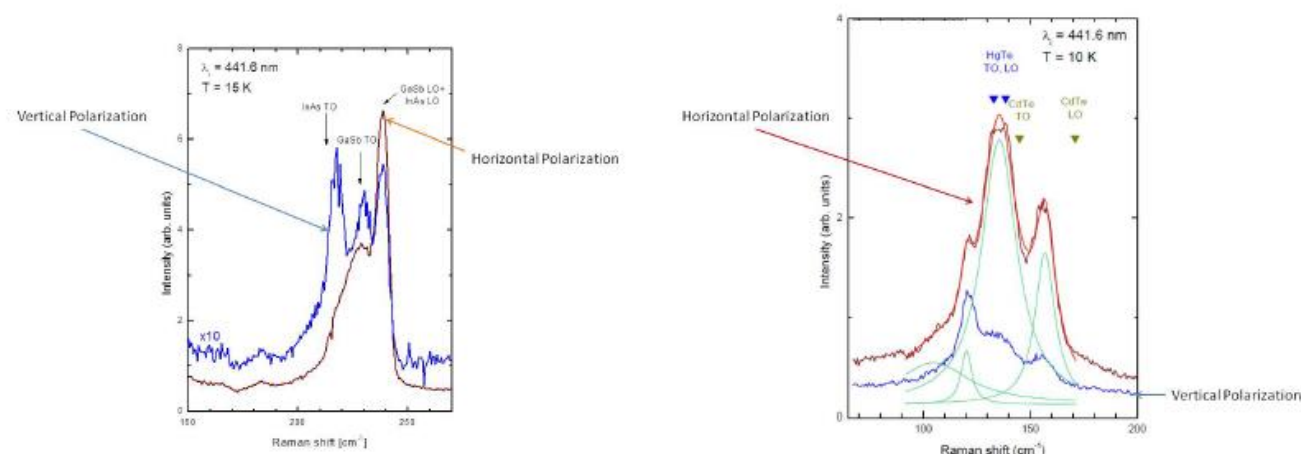


Figure 3.6 (a) Raman spectra of the SLS structure for two polarization configurations. (b) Raman spectra of MCT structure for two polarization configurations.

Night Vision Directorate provided Actoprobe LLC with two test structures possessing epitaxial structures comparable to real FPA material and having sidewall profiles similar to real FPA pixels. These two structures are representative of the most important FPA materials of interest to Night Vision Directorate. One of these structures is HgCdTe(MCT), the other is InAs-GaSb strained layer superlattice (SLS). We measured Raman spectra from MCT and SLS at low temperature in a closed-cycle Helium cryostat to obtain the highest possible signal-to-noise ratio. Two laser polarization configurations were utilized to identify Raman peaks for TO and LO phonons. Figure 3.4 shows Raman spectra of the SLS structure for incident and scattered light polarizations parallel and perpendicular to each other. The Raman shift for SLS structure is in the range of 200-250 cm^{-1} which is far enough from the laser line to be measured with a single grating Raman spectrometer. In contrast, the Raman shift for the MCT material is smaller (about 100-170 cm^{-1}), see Fig. 3.6, which would require a multiple-grating Raman spectrometer or holographic notch filter to measure. Also, the SLS structure gives a more intense Raman signal than the MCT for the excitation wavelength used (in the visible, blue-green range). This makes the SLS material a preferable choice for initial studies at room temperature.



Figure 3.7 FPA structure

3.3.3 Raman from real SLS FPA structure

We obtained a real SLS FPA structure from Skinfrared LLC (spin o_ from UNM) to investigate the possibility of characterizing pixel sidewalls with Raman spectroscopy. The FPA structure, shown in Fig. 3.7, is a dual-band LW/LWIR type II superlattice material. The pixels are formed by etching 6.7 µm through the epitaxial layers using ICP etching with BCl₃ chemistry. The experimental setup from Fig. 3.3 was applied to perform Raman characterization for this FPA. We aimed our study at detecting the difference between Raman spectra obtained from the pixel top (pixel center) and the pixel sidewall. The experimental results are shown in Fig. 3.8. The Raman signal from sidewalls was observed to be about two times smaller than that obtained from the top of the pixel. This difference can be explained by the poorer material quality on sidewalls resulting from etching damage compared to the unetched pixel top. A difference in material quality is also noticeable as Raman spectral broadening on sidewalls compared to the pixel top. Lorentzian fitting was performed to quantify the difference in Raman spectra as shown in Fig. 3.8.

3.4 Conclusion

Analysis of Raman spectra from a SLS FPA demonstrated that TO phonon peaks can be utilized for characterization of pixel sidewall quality. Raman peaks corresponding to both InAs and GaSb phonons carry information about material quality on pixel sidewalls. This information is contained in both peak intensity and full width at half maximum (FWHM). We can see that peak FWHM is increased (by 1.24 cm⁻¹ and 1.68 cm⁻¹ for InAs and GaSb phonons, respectively) at the sidewalls compared to the pixel top, likely due to defects introduced by the plasma etching process. Since both peak magnitude and FWHM are affected, the phonon intensity is characterized by the area under the Raman peak (integrated

intensity). The integrated intensity of the InAs peak is observed to decrease by 42% for InAs and 30% for GaSb on sidewalls, compared to the pixel top. This might suggest that InAs is more severely affected by the plasma etch than GaSb.

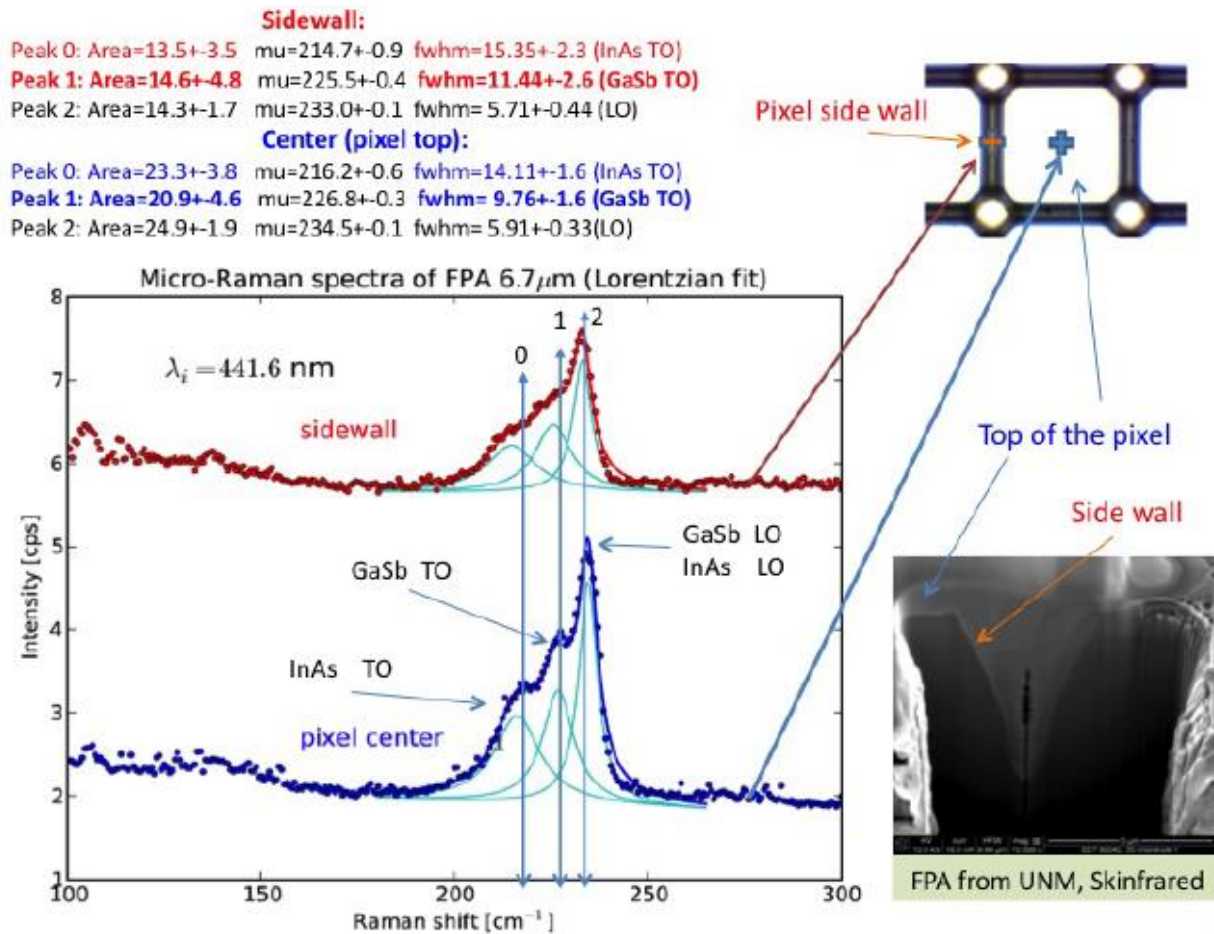


Figure 3.8 Experimental results for SLS-FPA structure.

In summary, we can conclude that Raman spectroscopy is a useful tool to characterize the pixel sidewalls, as was shown in the experiment above. In Phase II we will improve the signal-to-noise ratio and spacial resolution. As already mentioned in section 2.2 a Krypton Ion Laser will increase the interaction volume for Raman scattering because of its longer wavelength (647.1nm and 752.5 nm). A single grating Raman spectrometer (Renishaw) will improve the instrument throughput and therefore improve the signal-to-noise ratio. An objective with higher NA (0.85{0.95}) will increase the Raman signal collection and spatial resolution. Furthermore, an additional method to substantially improve the spatial resolution is TERS.

4 Progress in High aspect ratio AFM probe fabrication

To extract morphological information of FPA sidewalls, high-aspect-ratio (HAR) probes of very high quality are required. In this section, the HAR probes fabricated by Actoprobe are demonstrated and their imaging capability combined with extended Z-piezo is tested.

4.1 High aspect ratio probes fabricated by Actoprobe

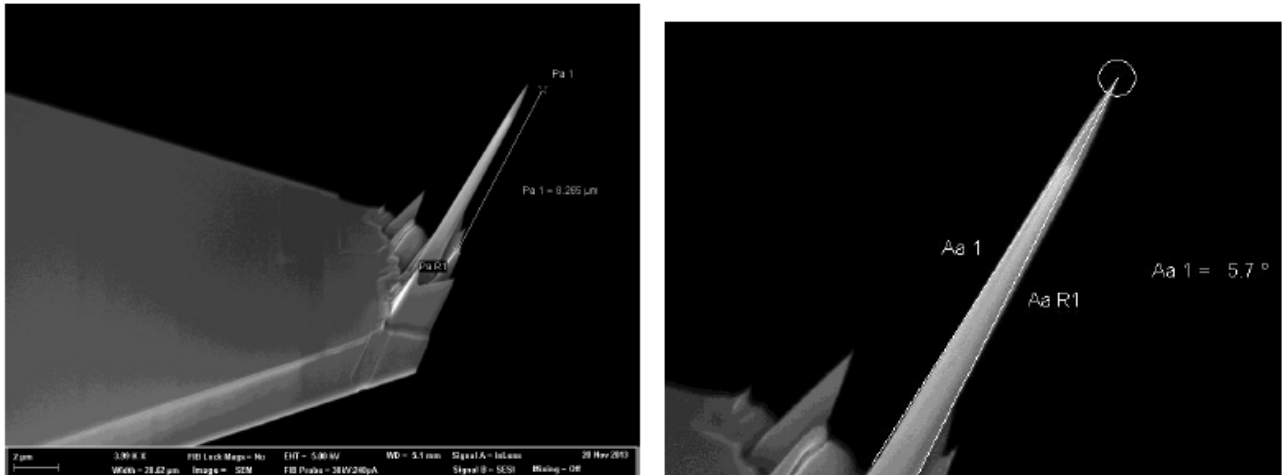


Figure 4.1 SEM image of high-aspect-ratio probe tips fabricated from AC240 Olympus probes.

Figure 4.1 shows high-aspect-ratio probes with a usable scanning length of approximately 8.25 μm , which were fabricated from AC240 Olympus probes. The aperture of the tip is 5.7°, which should allow scanning of samples with up to 87.1° steep walls. The tip radius of curvature is ~ 13 nm. The probes are tilted 15° with respect to the cantilever. This is to compensate for the cantilever angle when mounted in the AFM.

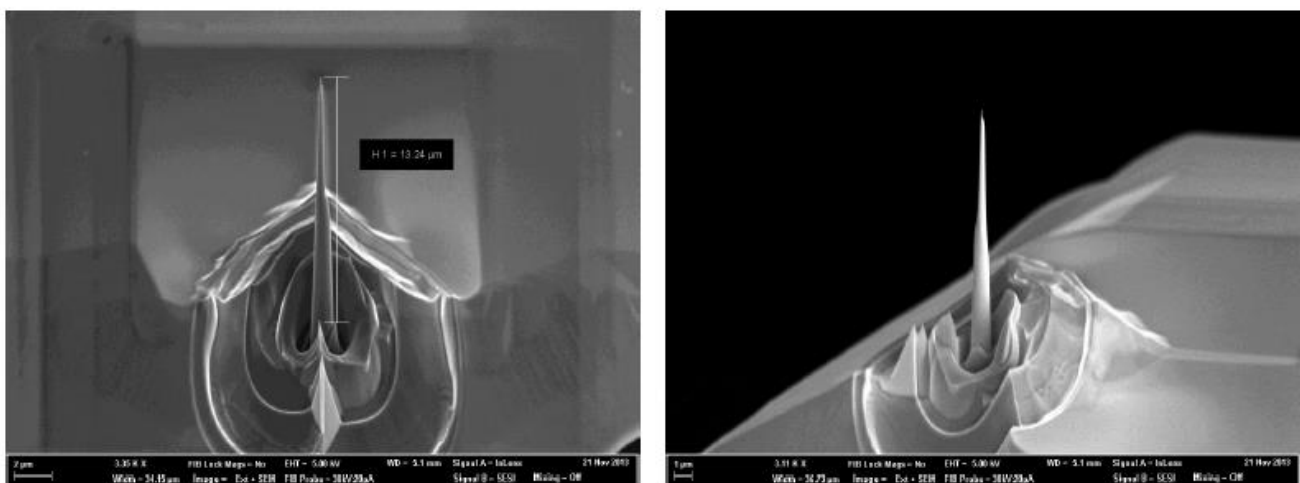


Figure 1 SEM image of high-aspect-ratio probe tips fabricated from PPP-NCRL Nanosensors™ probes.

ACTOPROBE LLC
801 University S.E., Suite 100, Albuquerque, New Mexico, 87106
Phone: +1 (505) 272-7176; Email: aukhanov@actoprobe.com;
www.actoprobe.com

Figure 4.2 shows high-aspect-ratio probes with a scanning length of approximately 13 μm that were fabricated from PPP-NCRL Nanosensors™ probes. The aperture of the tip is 6.7° , which should allow scanning of samples with 86.6° steep walls. The tip radius of curvature is $\sim 6\text{ nm}$, allowing high lateral resolution (atomic resolution). The probes were fabricated in several steps: First the total length of the tip is defined. Then a region of about $7\mu\text{m}$ with an aperture angle of less than 5.7° is defined. Subsequently a region of $\sim 6\mu\text{m}$ towards the contact region between the tip and the cantilever is defined with an aperture of less than 7° . This is to maintain the robustness of the tip if used for very steep and high walls. Finally, the cantilever is cut such that the tip is positioned at its very end. This insures good alignment of the AFM's laser spot to the tip, which is important to maintain a very good lateral resolution while scanning very tall structures. Due to the critical dimensions, this tip was not tilted with respect to the cantilever.

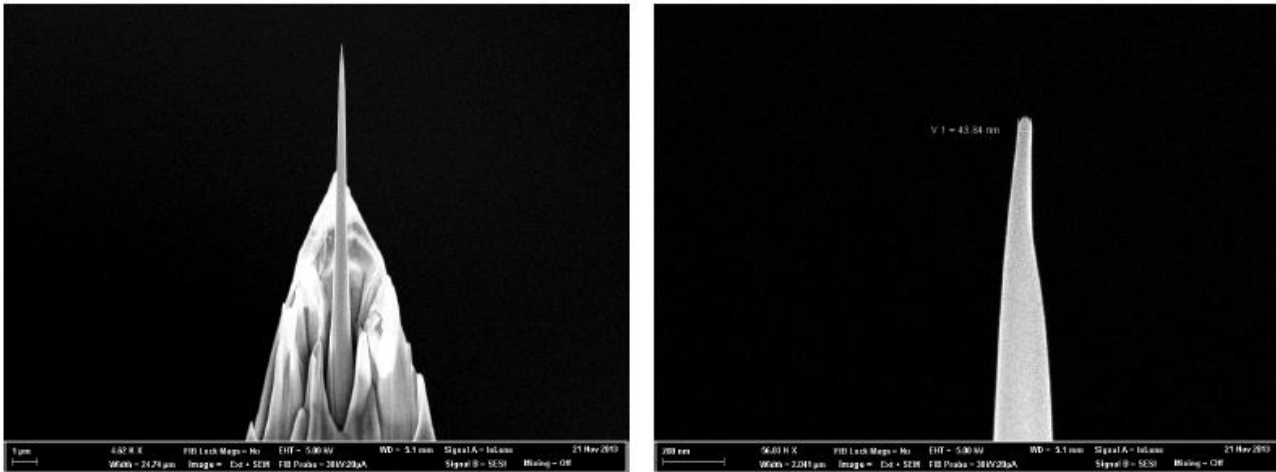


Figure 2 SEM image of high-aspect-ratio probe tips fabricated from TR-400 Olympus probes

Figure 4.3 shows probes with a scanning length of approximately 10 μm , fabricated from TR400 Olympus probes. The probes were coated with Pt to work in non-contact electric mode. The metal coating also serves as a test for fabricating metal coated tips for enhanced Raman spectroscopy. The aperture of the tip is 6° , which should allow scanning samples with 87° steep walls. The tip radius of curvature is $\sim 40\text{ nm}$. This large radius is due to the Pt coating. The probes are tilted 15° with respect to the cantilever, to compensate for the cantilever angle, when mounted in the AFM.

In summary, high-aspect-ratio tips were fabricated from Si probes using a Zeiss Auriga Ga ion beam. All probes were designed for non-contact AFM scanning mode. Tips have been fabricated for scan heights between 8 and 13 μm , capable of scanning up to 87° steep walls, with 6nm tip radius of curvature to provide atomic resolution. The tips can be tilted with respect to the cantilever to compensate for the cantilever angle when mounted in the AFM. The tips can also be coated with Pt to facilitate electrical scans and to reinforce the mechanical contact between the cantilever and the tip.

4.2 Probe testing with extended Z-piezo

Imaging a complete height profile of a $\sim 10\mu\text{m}$ deep trench requires an AFM scanner with extended vertical range. Actoprobe was able to make such images using an AFM with an extended Z-Range Head Retrofit (HD-ACC-EXTZ-R) from Asylum Research Inc. (Oxford Instruments, Santa Barbara, CA), that features a $40\mu\text{m}$ vertical range. Figure 4.4 shows an SLS test-sample (from Night Vision Inc., Pasadena, CA) with the AFM probe as seen through an optical microscope along with height profiles. These were obtained using the extended scanner and a high-aspect-ratio probe with a $\sim 10\mu\text{m}$ long tip, that was fabricated by Actoprobe (see Figure 4.1). The height profiles show a $\sim 9.2\mu\text{m}$ deep trench that is 10 -

ACTOPROBE LLC

801 University S.E., Suite 100, Albuquerque, New Mexico, 87106

Phone: +1 (505) 272-7176; Email: aukhanov@actoprobe.com;

www.actoprobe.com

13 μm wide. The 28 μm scan height profile shows the entire trench, with a step at the left sidewall. A 5 μm scan height profile shows the left sidewall in higher resolution and confirms the presence of the step.

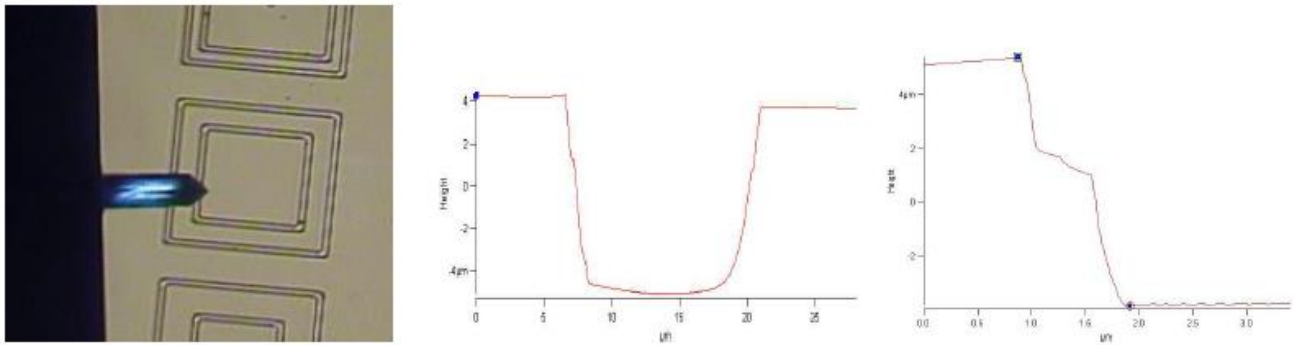


Figure 4.4 The SLS test sample (Night Vision Inc.) with the AFM tip (left) as seen through an optical microscope. Height profile of this SLS test sample associated with the scans in Figure 4.5. The 28 μm scan (center) shows the entire trench. On the right, there is a height profile of a 5 μm scan that shows the left sidewall in higher resolution and detail.

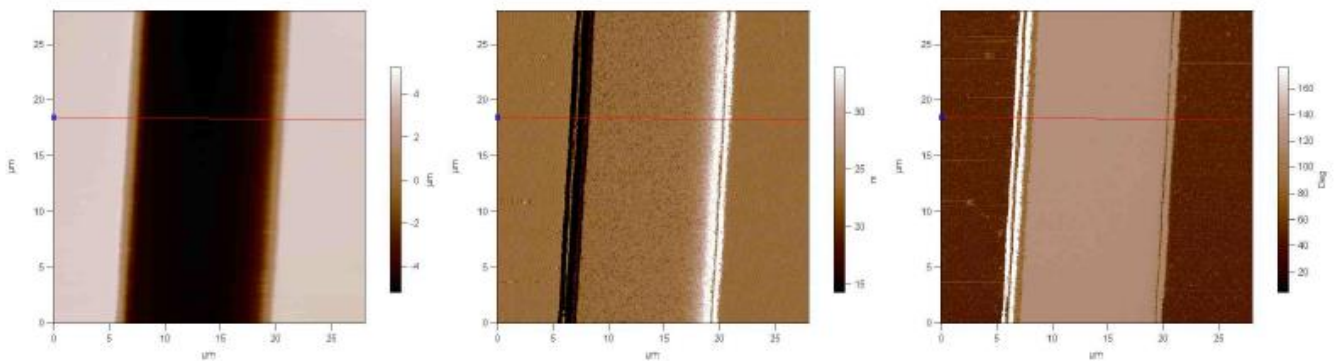


Figure 4.5 SLS test sample (Night Vision Inc.): 28 μm AFM scans over the entire trench using a scanner with extended vertical range (40 μm) and the high-aspect-ratio probe tip with $\sim 10\mu\text{m}$ length fabricated by Actoprobe. Topography scan (left), amplitude (center) and phase map (right).

Figure 4.6 shows a 28 μm AFM scan of this SLS test sample (topography, amplitude and phase) and Figure 33 shows a more detailed analysis of the left sidewall in a 5 μm scan and a 2.5 μm scan as well as a 3D representation. Figure 4.7 shows an amplitude and phase scan associated with the 2.5 μm scan, that reveal more details of the step in the left sidewall.

In the 28 μm height profile in Figure 31 center, there is a difference between the left and right sidewall. The difference may be actually present in the sample or it may be an artifact of the AFM scan. The latter may be due to a small angle between the probe tip and the sidewall, which results in a true image of only one sidewall and a slightly distorted one of the other. Whether difference is present in the sample or is due to an AFM artifact, can be determined from AFM scans with the sample rotated by 180 degrees. If the shape differences of the sidewalls follow the sample rotation, then the sidewalls are actually different, whereas if the shapes switch from one to the other sidewall, then they are due to an AFM artifact.

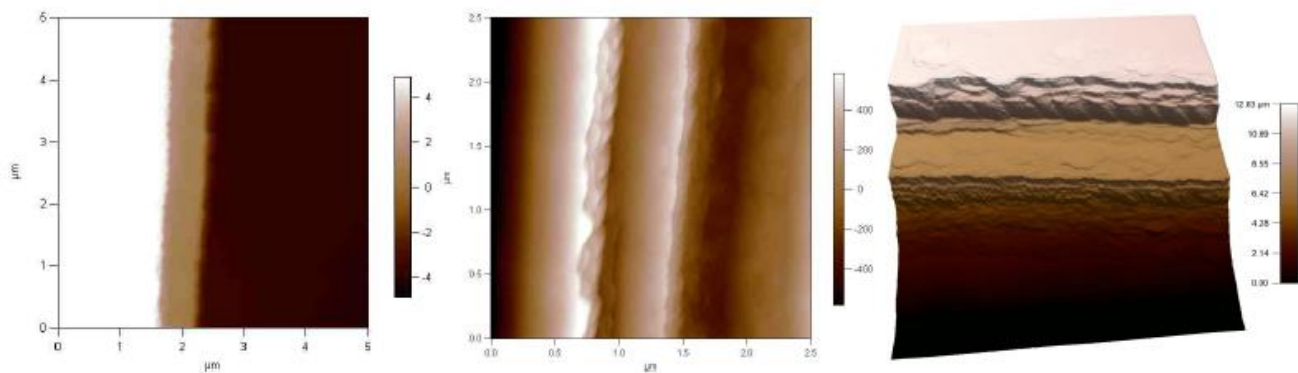


Figure 4.6 SLS test sample (Night Vision Inc.): Higher resolution scans of the left sidewall. The 5 μ m topography scan (left) shows the step at \sim 3-4 μ m below the top, as shown also in the height profiles in Figure 31. The 2.5 μ m scan (center) shows the step in more detail, but the height scale is tilted due to flattening. On the right, there is a 3D image of the left sidewall with a correct height scale. It also shows the step.

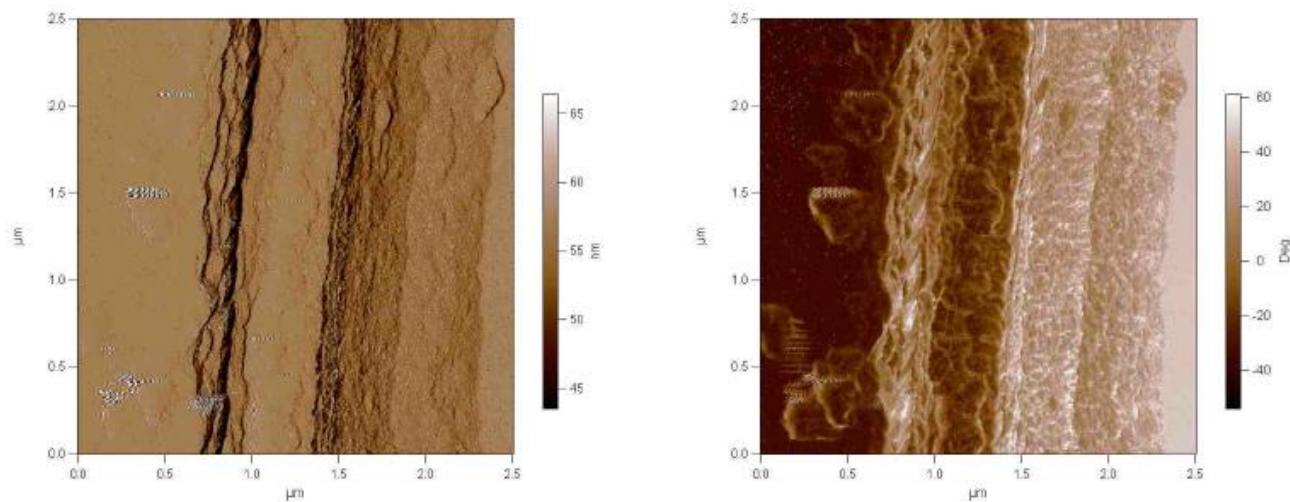


Figure 4.7 SLS test sample (Night Vision Inc.): Higher resolution scans of the left sidewall. Amplitude (left) and Phase map (right) associated with the 2.5 μ m scan in Figure 33 center. These images show more details of the step in the left sidewall.

4.3 AFM Scans on FPA Samples from SKinfrared and NVESD

4.3.1 SKinfrared sample

Fig. 4.8 shows a 20 μ m AFM scan of this FPA sample from SKinfrared compared with SEM image. The trench depth is about 7.2 μ m. The 3D image reconstructed using the data from AFM scan shows perfect match to the image obtained from SEM as seen in Fig. 4.9. A close-up scan at the corner (Fig. 4.10) and trench (Fig. 4.11) clearly shows roughness changing along the sidewall due to etching.

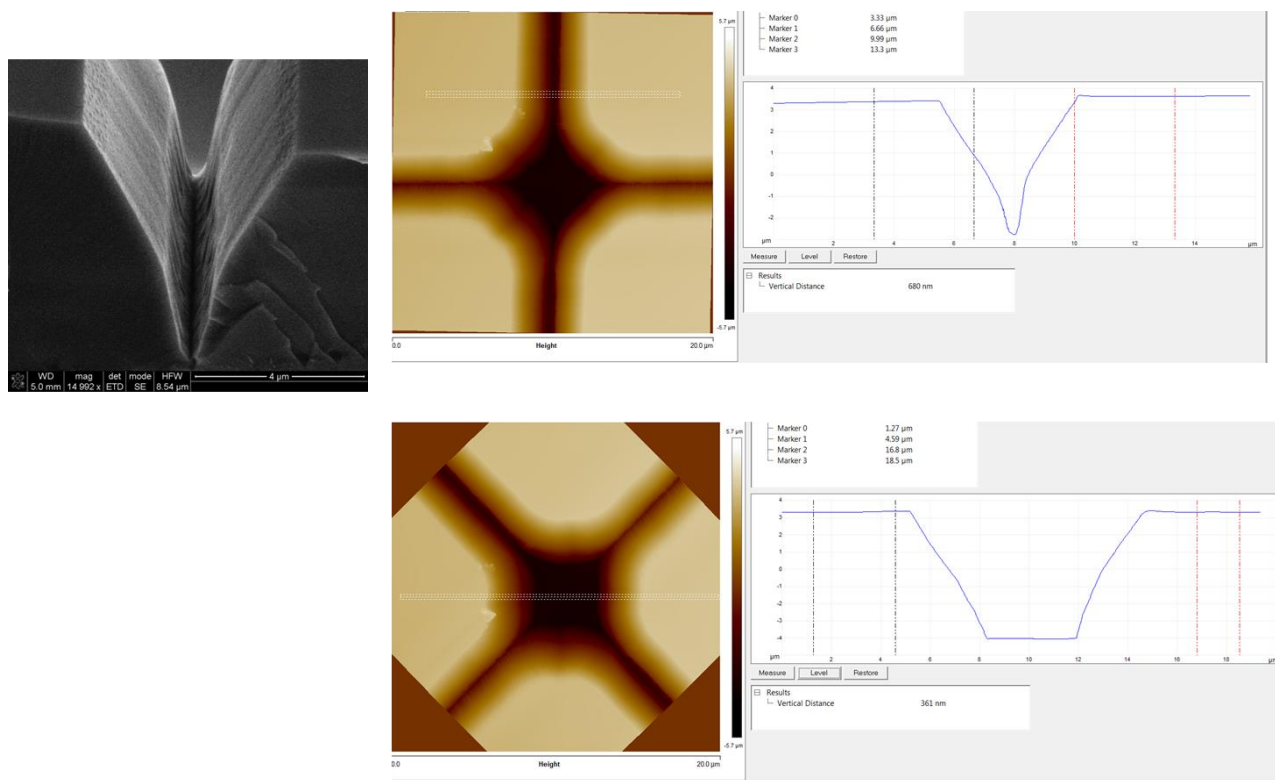


Figure 4.8 SEM (left) and AFM scan (right) on SKInfrared FPA measured with HAR probe

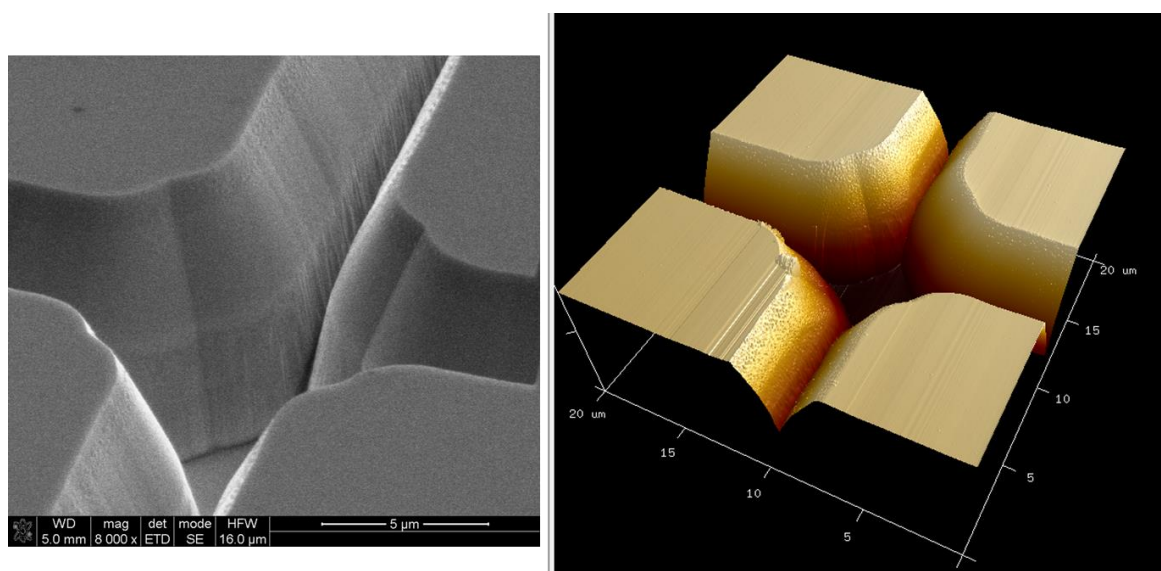


Figure 4.9 SEM (left) and AFM 3D image (right) of SKInfrared FPA measured with HAR probe

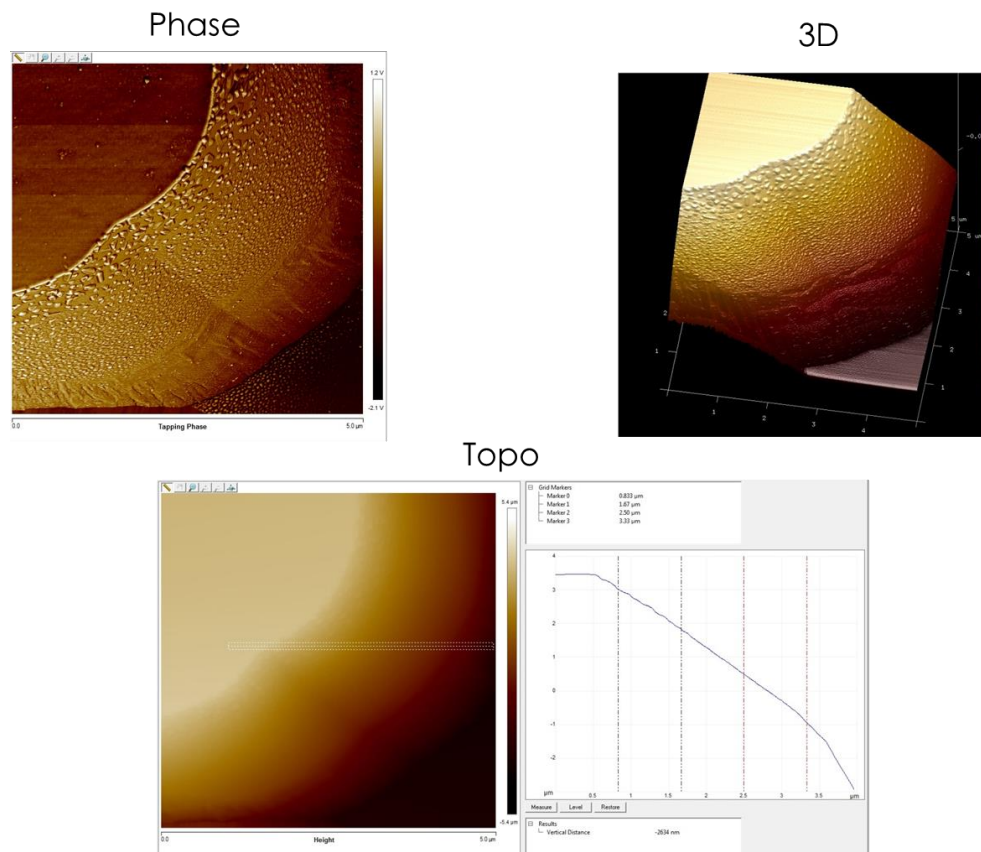


Figure 4.10 AFM image on the corner of SKInfrared FPA Measured with HAR Probe, 5x5μm

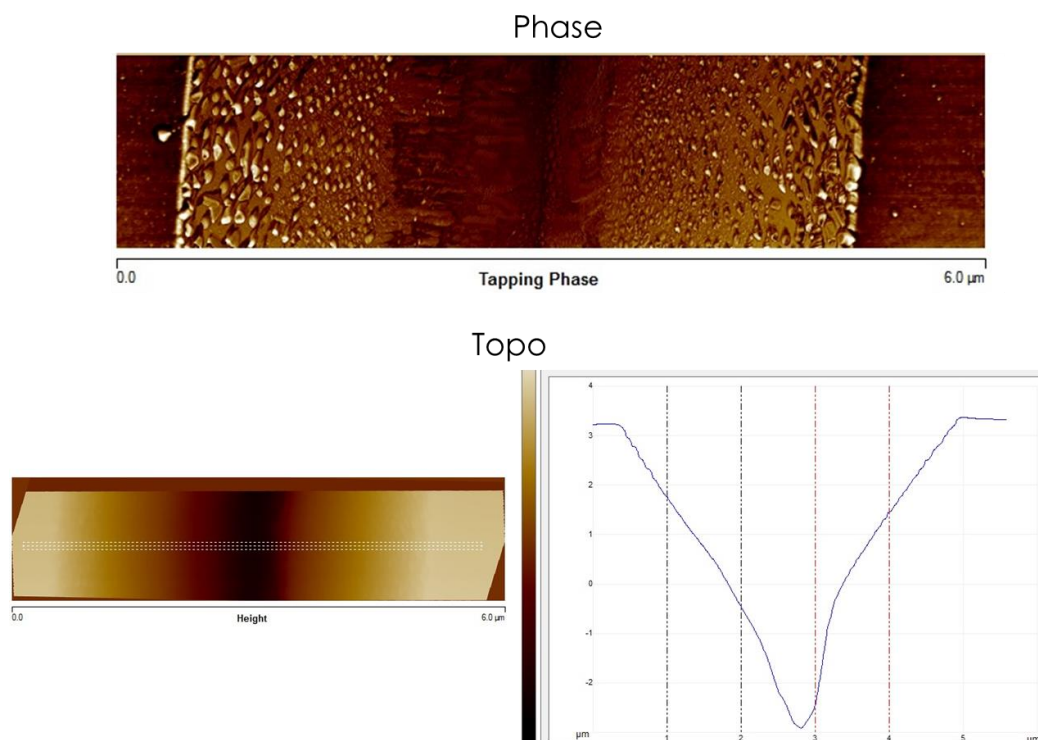


Figure 4.11 AFM scan across the gap on SKInfrared FPA Measured with HAR Probe 1x6μm

ACTOPROBE LLC
 801 University S.E., Suite 100, Albuquerque, New Mexico, 87106
 Phone: +1 (505) 272-7176; Email: aukhanov@actoprobe.com;
www.actoprobe.com

4.3.2 NVESD sample

An FPA sample from NVESD is scanned using HAR probe as shown in Fig. 4.12 with a scan width of 10 μ m \times 10 μ m. The trench has a depth of about 6.5 μ m. The fine features on top, sidewall and bottom of the sample are obvious in the AFM scan. Fig. 4.13 is a higher-resolution 5 μ m \times 5 μ m scan across the trench with more details on the sidewall. To compare the surface roughness at different depth on the sidewall, small area scans are performed at three consecutive sections and the results are shown in Fig. 4.14.

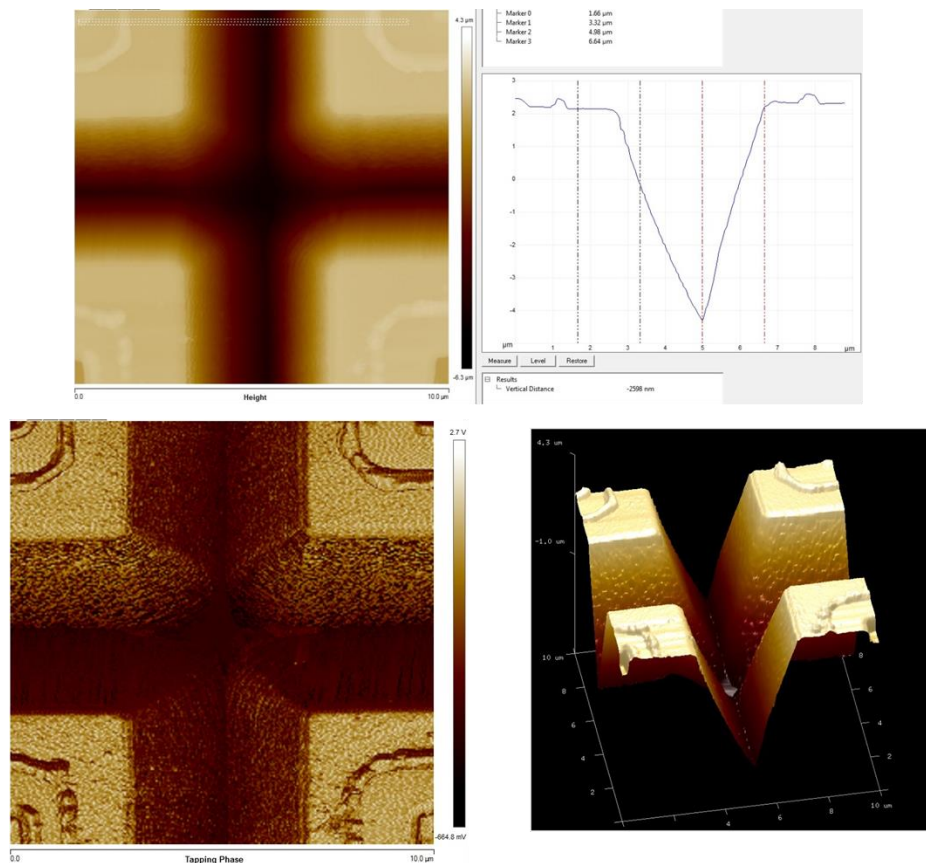


Figure 4.12 AFM scan on NVESD FPA – 10 \times 10 μ m, 256 \times 256

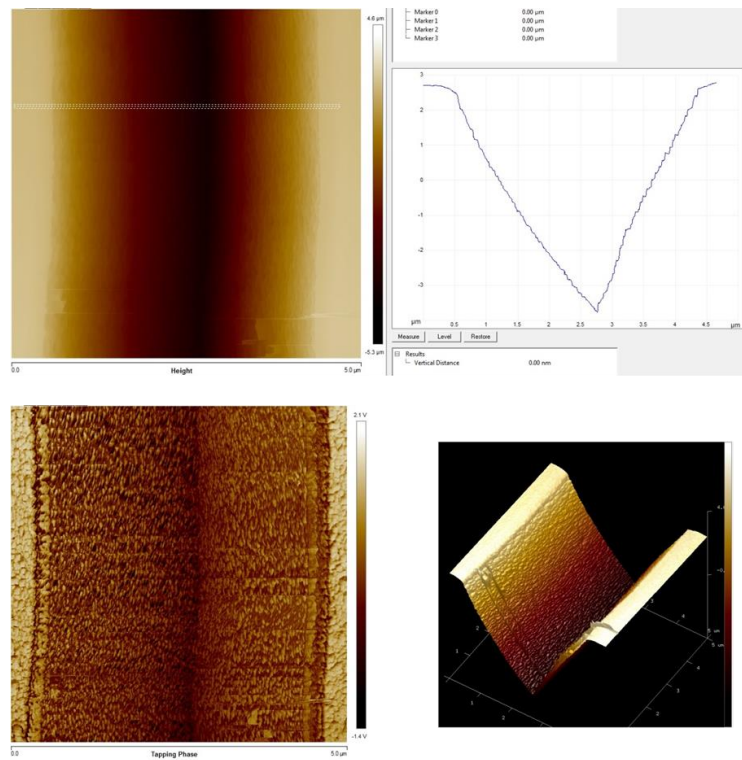


Figure 4.13 AFM scan across the gap on NVESD FPA – 5x5um, 1024x1024

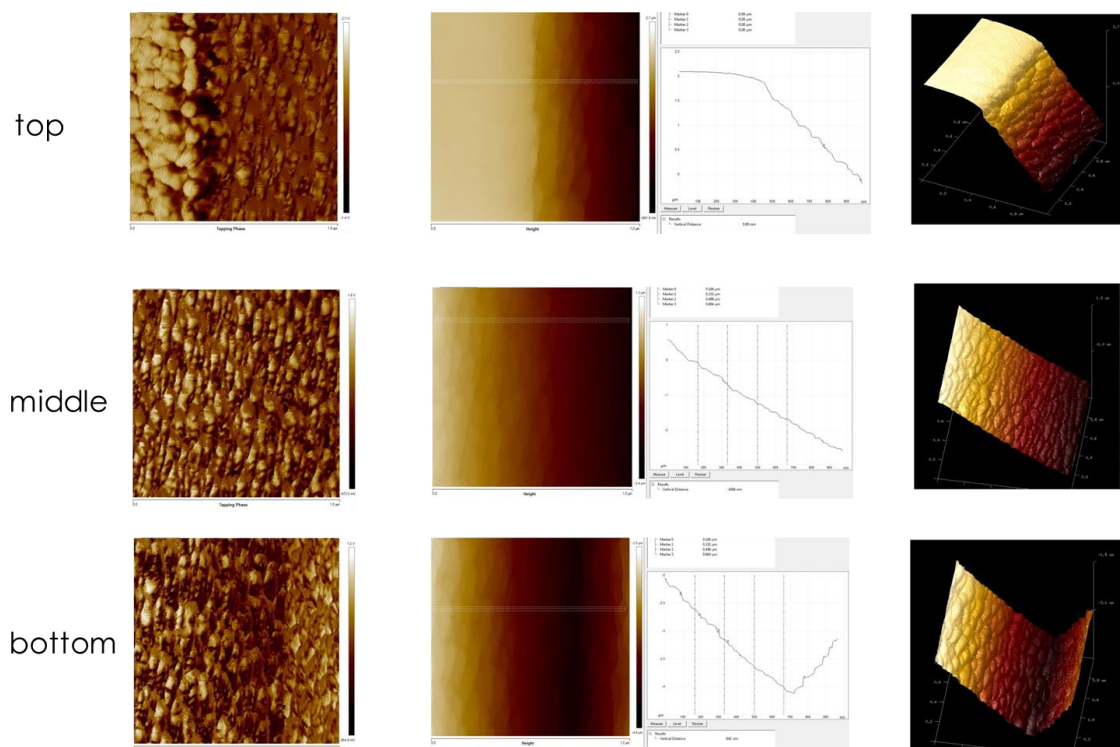


Figure 4.14 More detailed AFM scan on the sidewall of NVESD FPA – trench, 1x1um, 256x256

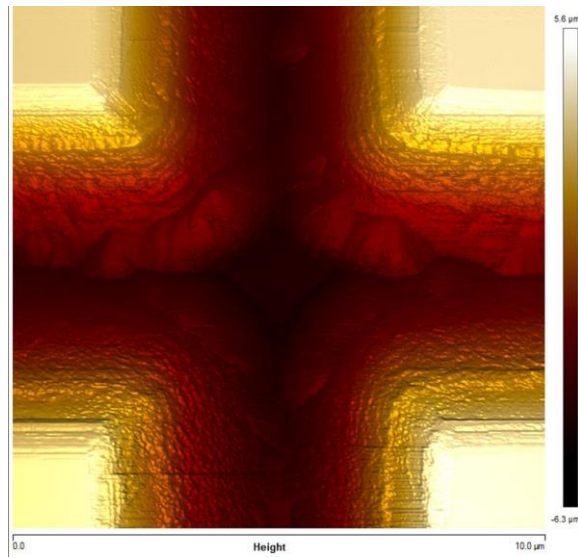


Figure 4.15 BS6 Night Vision FPA AFM Image

5 Future Upgrades and Accessories

5.1 AFM Active Optical Probe(AAOP):

AAOP is fabricated on a III-V substrate and combines diode laser and detector inside the AFM probe (Fig. 5.1). Therefore, no external laser excitation is required for TERS and NSOM.

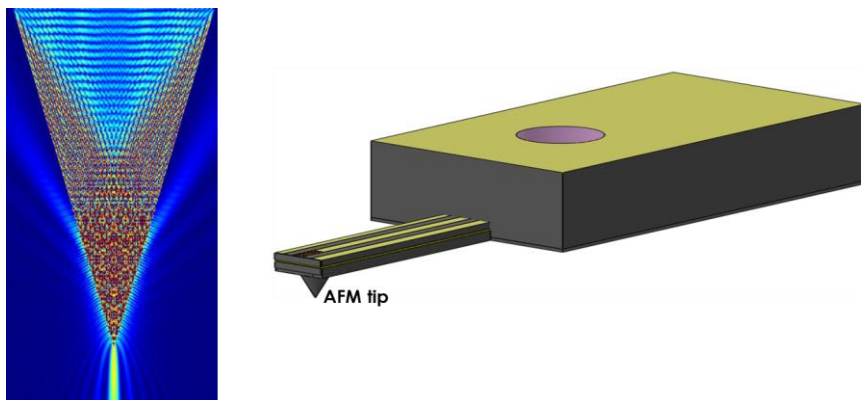
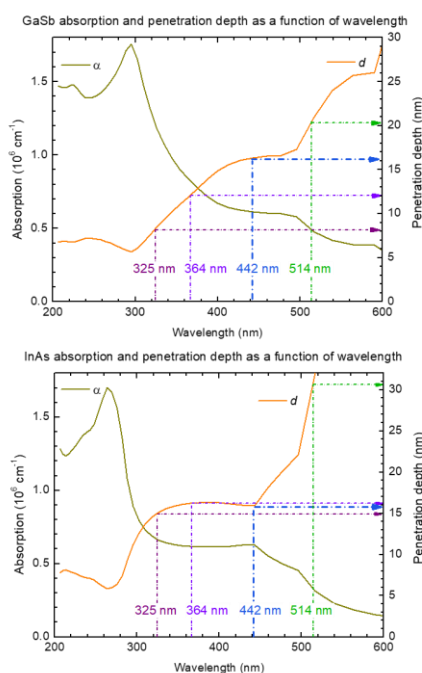


Figure 5.1 AFM Active Optical Probe for FPA characterization

5.2 Additional Raman lasers: UV, blue, green, infrared

As shown in Fig. 5.2 and Fig. 5.3, lasers of different wavelengths can be used for extracting Raman information at various depth from the surface of the sample. More surface sensitivity is obtained with shorter wavelength. Furthermore, as discussed in Section 2.2 and Fig. 5.4, for an FPA sample NSOM images at different laser wavelengths result in different fringe patterns and can be used to derive the material composition.



Raman micro-spectroscopy on FPA arrays: excitation using 441.6 vs 514.5 nm

- ❖ Green laser (514.5 nm):
Information depth ~20 nm
→ expect more bulk-like spectra
- ❖ Blue laser (441.6 nm): shorter information depth → expect increased contribution of near surface regions
- ❖ Using UV excitation can decrease the information depth in GaSb down to ~4nm (325 nm laser) ⇒ more surface sensitivity
However, the microscope needs to be upgraded with the UV optics.

Data from D. E. Aspnes and A. A. Studna, *Phys. Rev. B* 27, 985-1009 (1983)

ACTOPROBE LLC

801 University S.E., Suite 100, Albuquerque, New Mexico, 87106

Phone: +1 (505) 272-7176; Email: aukhanov@actoprobe.com;

www.actoprobe.com

Figure 5.2 Excitation with Raman lasers of different wavelength

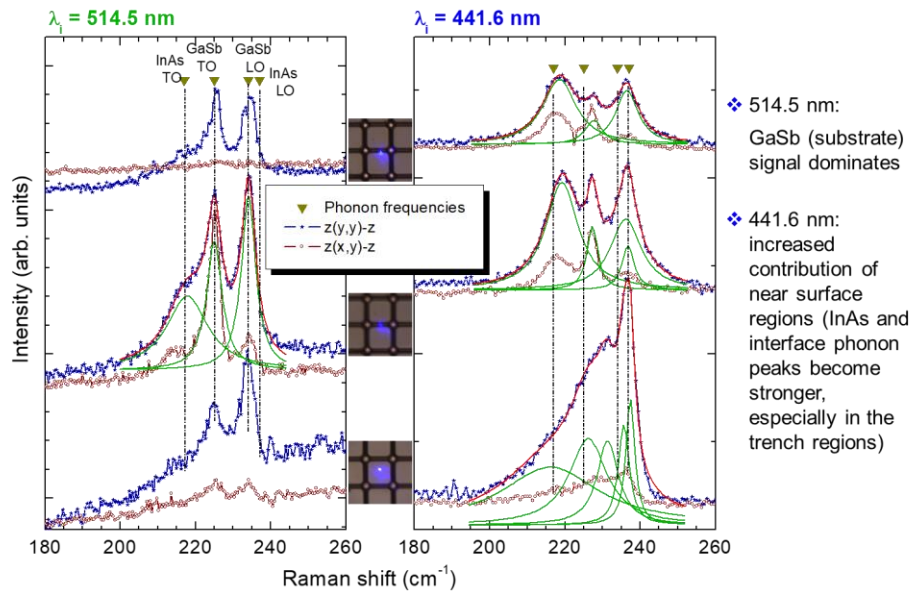


Figure 5.3 Raman micro-spectroscopy on FPA arrays: excitation using blue (441.6 nm) vs green (514.5 nm) lasers

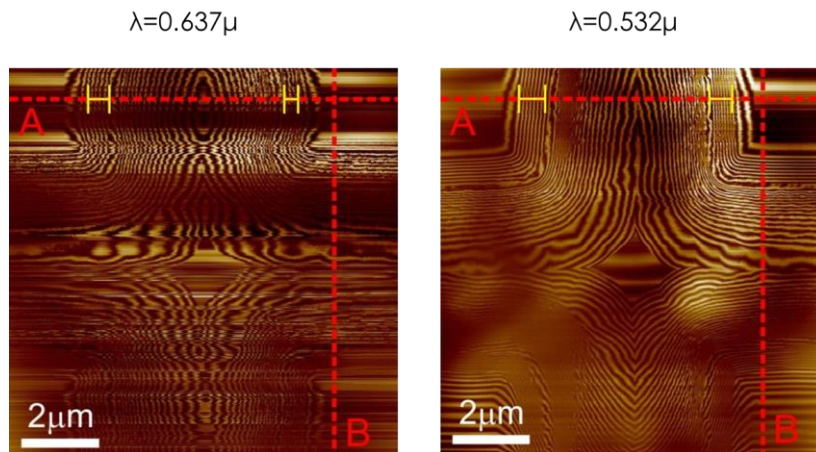


Figure 5.4 Additional Raman lasers: UV, blue, green, infrared

5.3 Fast confocal scanning

Fast confocal scanning microscopy (Fig. 5.5) can be used to reconstruct the optical and Raman information from a much larger area on the sample. For example, Fig. 5.6 shows a stitched 2.6mm x 3.6mm image consisting of 5 μm x 5 μm scans. This is very useful for applications such as defect mapping (Fig. 5.7) and 3D mapping (Fig. 5.8)

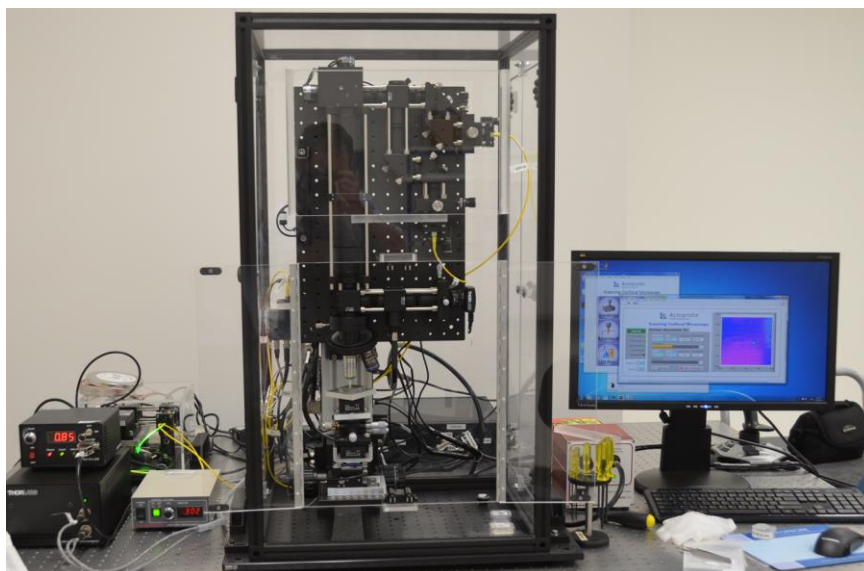


Figure 5.5 Scanning Confocal Microscope (SCM) for FPA characterization

Stitched image(58x72 subimages, each 512x512)

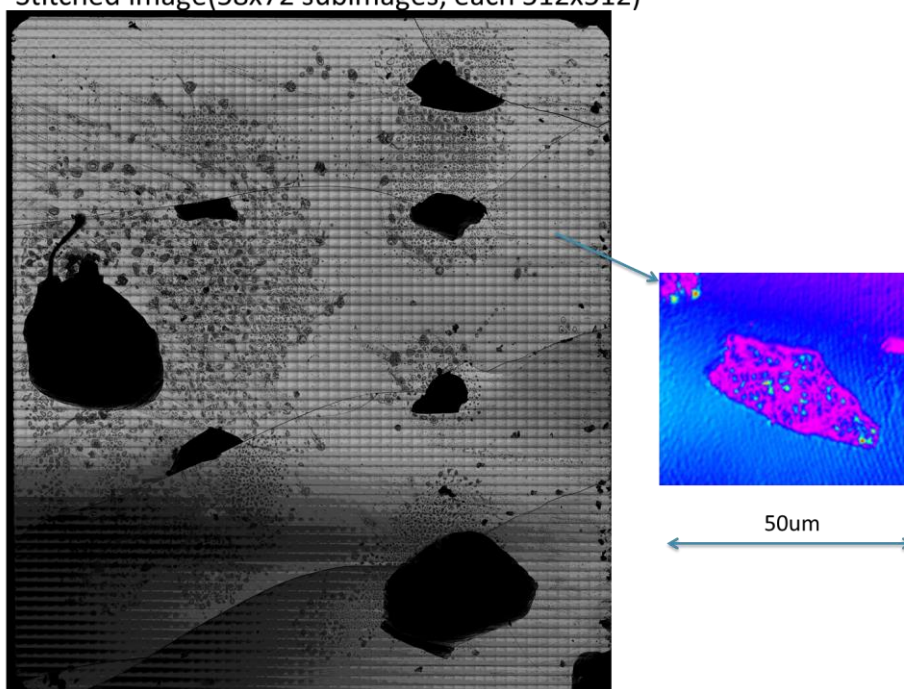


Figure 5.6 Stitching of SCM images

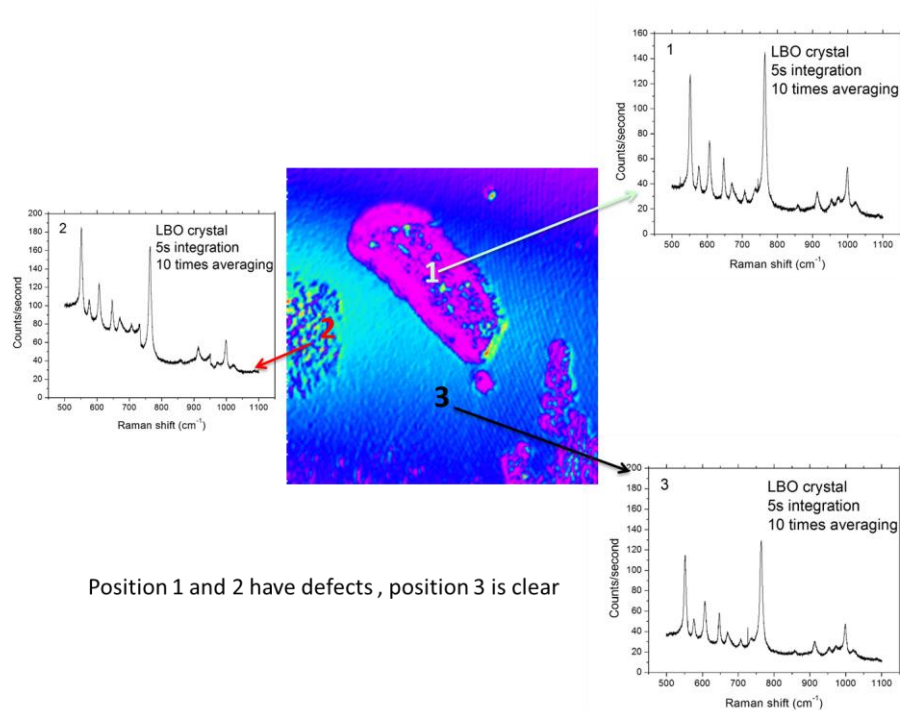


Figure 5.7 SCM for defect identification

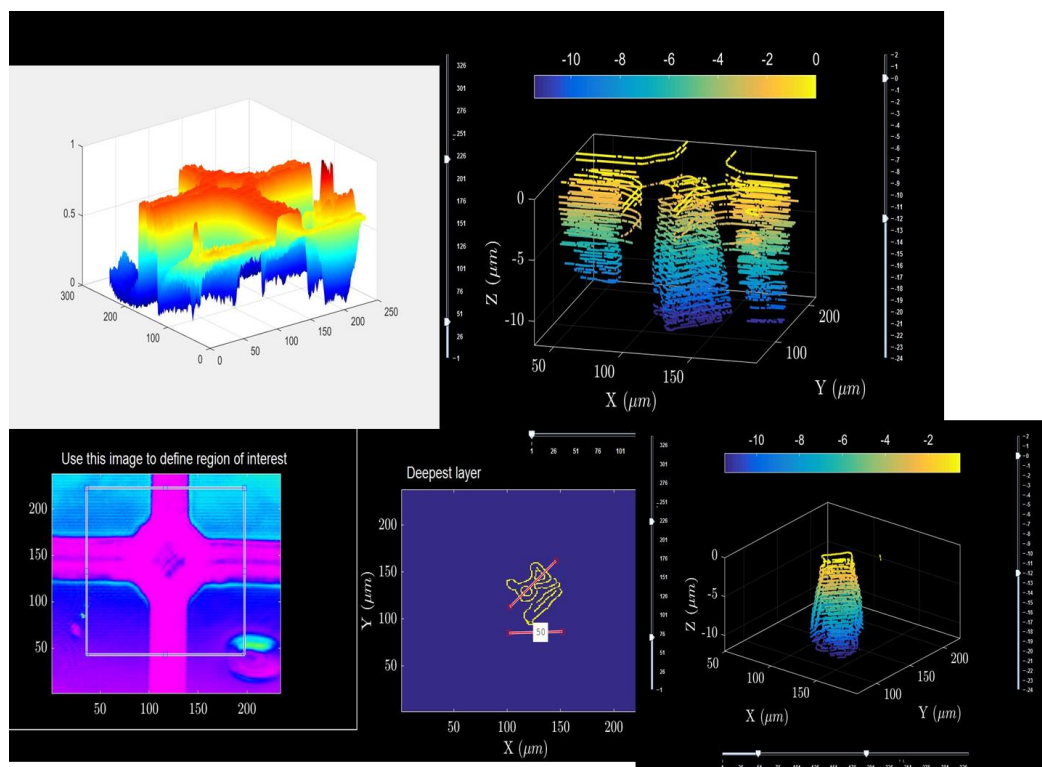


Figure 5.8 3D Mapping

5.4 Custom High NA objectives and Upright microscope configuration to increase Raman signal

With upright configuration (Fig. 5.9 and Fig. 5.10), diffraction-limited microscope objective can be used, with a dry numerical aperture of 0.95 and up to 1.3 in immersion oil. As a result, the laser can be focused four to ten times smaller.

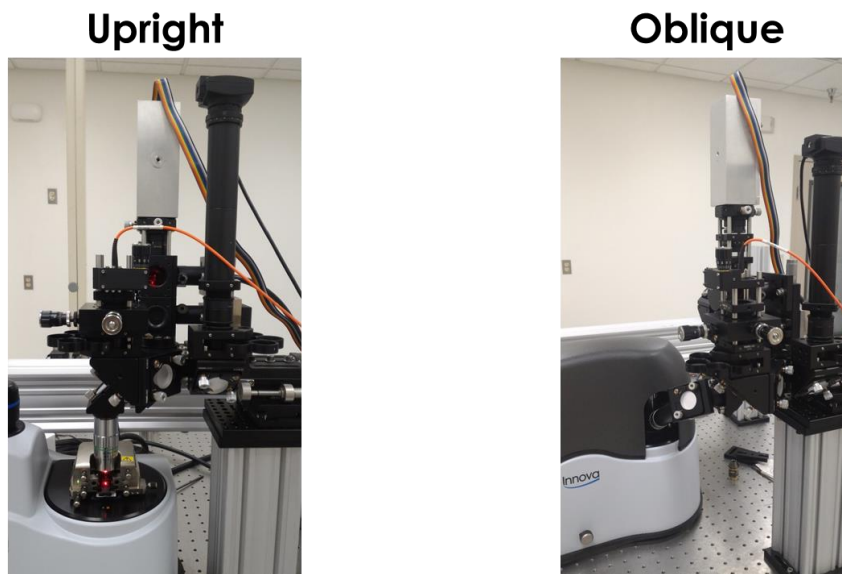


Figure 5.9 Microscope configurations

Upright and Oblique TERS Setup

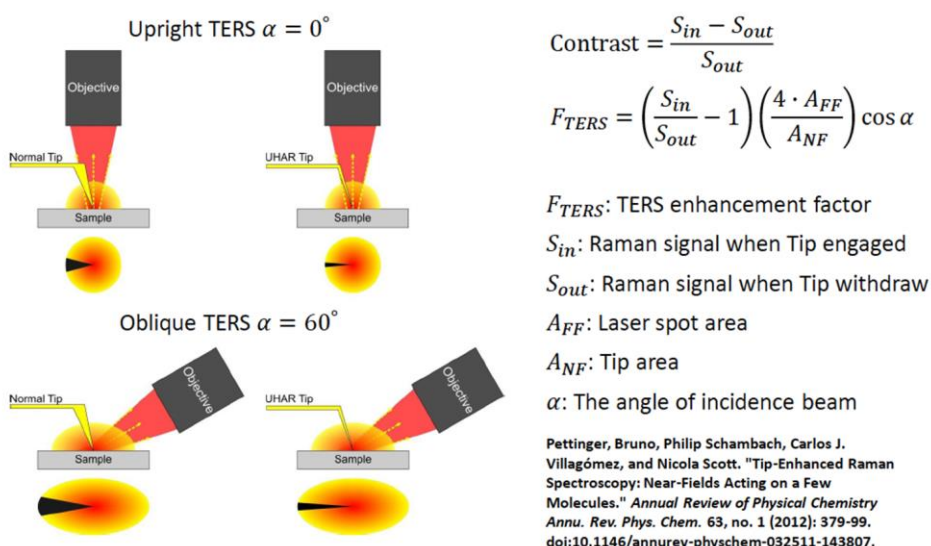


Figure 5.10 Comparison between upright and oblique configurations

5.5 Additional collection channel for NSOM imaging and Raman imaging at the same time

The current setup can be modified to have an additional channel for NSOM collection as shown in Fig. 5.11. Both NSOM and Raman imaging can be obtained in the same scan (Fig. 5.12).

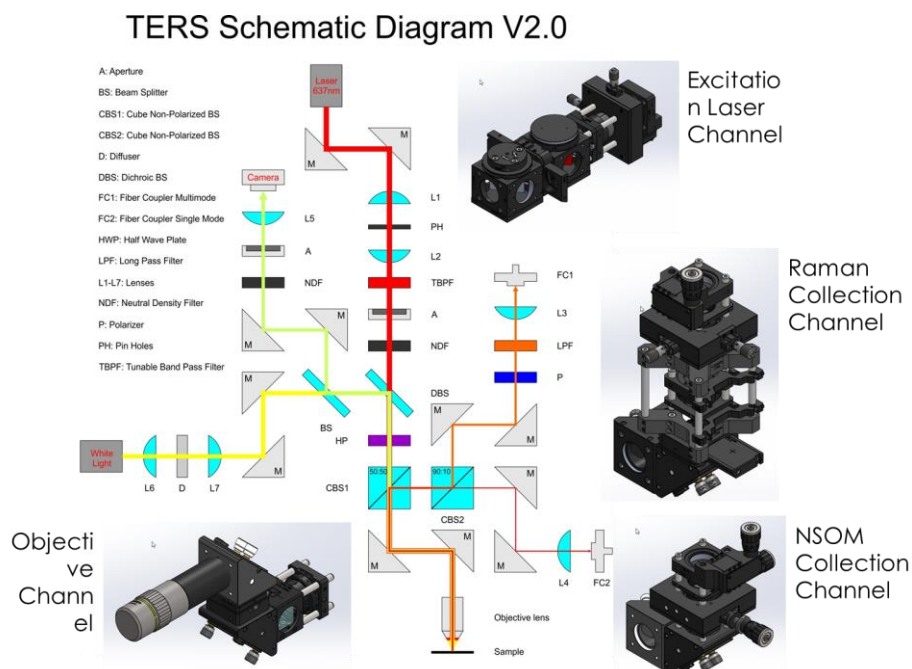


Figure 5.11 Setup schematic with additional NSOM collection channel

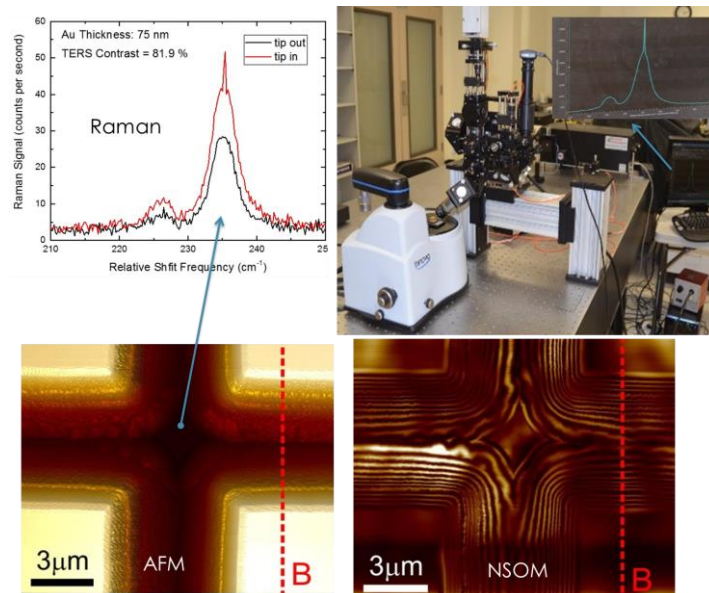


Figure 5.12 NSOM imaging and Raman imaging at the same time

5.6 TERS probe development for improving consistency and enhancement

A more systematic development of UHAR tapping mode probe can be conducted to determine the optimal geometry of the tip apex for TERS enhancement. Development of UHAR tuning fork and STM probes will require extensive research as well.

5.7 Polarization contrast

Raman spectroscopy on the sidewall depends on the polarization of the laser (Fig. 5.13) and the selection rules as explained in the slides in Fig. 5.14 and Fig. 5.15. In Fig. 5.16 and Fig. 5.17, FPA Raman spectra polarization dependence is investigated experimentally for both excitation geometries, oblique and upright, to the FPA surface and strongly suggest that for FPA studies perpendicular polarization (yz) is more preferable.

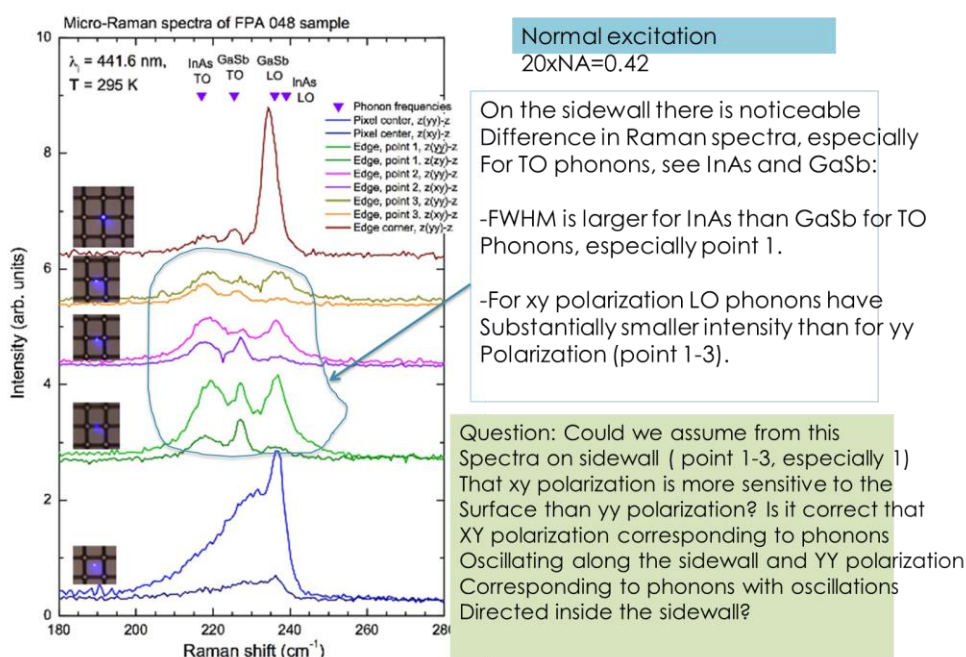


Figure 5.13 Polarization dependence of micro-Raman spectra

Raman micro-spectroscopy on FPA arrays

Raman selection rules and polarization selectivity

Raman scattering intensity I_s : $I_s \sim |\mathbf{e}_s \cdot \mathbf{R} \cdot \mathbf{e}_i|^2$

$\mathbf{e}_i, \mathbf{e}_s$ - unit vectors of polarization
of incident and scattered light

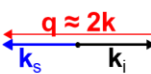
\mathbf{R} - Raman tensor
(tabulated for all crystallographic symmetry groups)

Also, energy conservation:

$\hbar\omega_i = \hbar\omega_s \pm \hbar\Omega$ - determines Raman shift (peak position in spectra)

and momentum conservation: $\mathbf{k}_i = \mathbf{k}_s \pm \mathbf{q}$

- determines the magnitude and direction of phonon wavevector \mathbf{q}

Backscattering: 

Polarization selection rules

Our case: cubic zinc-blebde-type crystals (GaSb, InAs)

- Group theory: phonons can have A_1 , E_1 or E_2 symmetry
- Superlattice grown in (001) direction (z): symmetry reduces to tetragonal
- Phonon have A_1 , B_2 , and E symmetry.

Corresponding Raman tensors:

$$R_{A_1}(z) = \begin{pmatrix} a & 0 & 0 \\ 0 & a & 0 \\ 0 & 0 & b \end{pmatrix} \quad R_{B_2}(z) = \begin{pmatrix} 0 & c & 0 \\ c & 0 & 0 \\ 0 & 0 & 0 \end{pmatrix} \quad R_E(x) = \begin{pmatrix} 0 & 0 & d \\ 0 & 0 & 0 \\ d & 0 & 0 \end{pmatrix}$$

$$R_E(y) = \begin{pmatrix} 0 & 0 & 0 \\ 0 & 0 & e \\ 0 & e & 0 \end{pmatrix}$$

Backscattering from (001) surface (e. g. center of a pixel):

$\mathbf{e}_i, \mathbf{e}_s$ have x,y components only, phonon wavevector $\mathbf{q} \parallel z$
 $\Rightarrow A_1$ and B_2 are LO phonons - active in Raman scattering,
 TO phonons have E symmetry and are not active

Figure 5.14 Raman selection rules and polarization selectivity

Excitation at the side wall:

- Due to large index of refraction ($n \approx 3.9$) for both InAs and GaSb, light enters the structure at angle $\approx 30^\circ$ from the layers plane \rightarrow large parallel component of \mathbf{q} (along (110) direction)
- Light polarization vectors \mathbf{e}_i , \mathbf{e}_s have components both along and perpendicular to the surface \rightarrow TO phonons become Raman active
- LO phonons involve vibrations mostly normal to the surface – less sensitive to surface defects
- TO phonons polarized parallel to the surface, along $(\bar{1}10)$ direction, may be more sensitive to the surface defects
- **However**, it is important to note, that most of the signal comes from the areas away from the surface (excitation depth ≈ 8.5 nm) \Rightarrow need to increase surface sensitivity:
 - use UV light \rightarrow shorter penetration depth
 - **TERS**

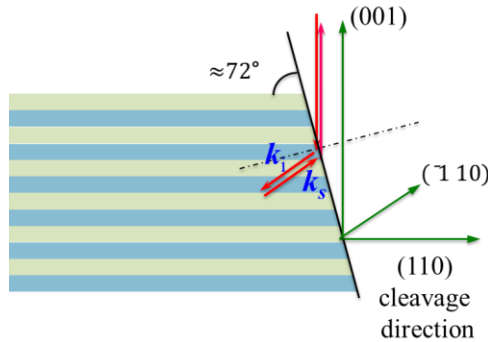


Figure 5.15 Polarization selection rules

Raman micro-spectroscopy on FPA arrays Polarized Raman spectra analysis

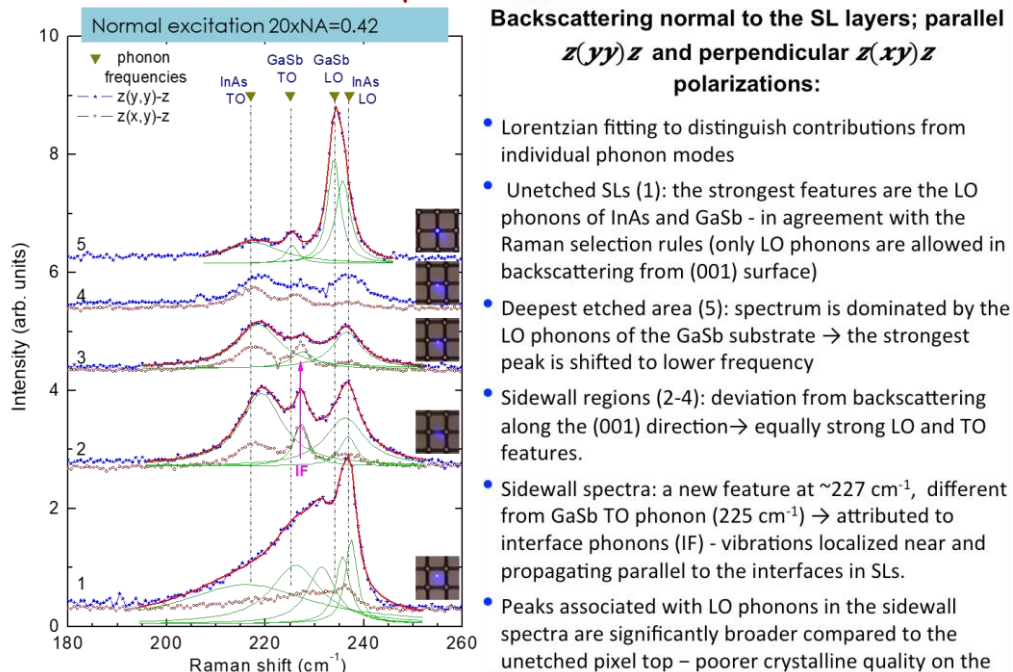


Figure 5.16 Raman micro-spectroscopy on FPA arrays with upright configuration

ACTOPROBE LLC

801 University S.E., Suite 100, Albuquerque, New Mexico, 87106

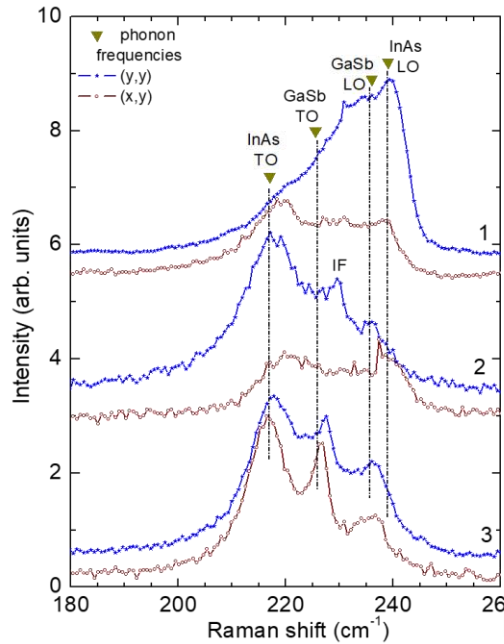
Phone: +1 (505) 272-7176; Email: aukhanov@actoprobe.com;

www.actoprobe.com

Oblique geometry:

Oblique excitation 20xNA=0.42

- excitation at $\sim 60^\circ$ with respect to the vertical axis z , (normal to the SL layers)
- collection along z axis in parallel $z(yz)$ and perpendicular $z(xy)$ polarizations



Numbers indicate the location of laser spots:

1 – unetched pixel center

2, 3 – sidewall regions

- The spectra are generally similar to those in backscattering along (001)

- The peaks of TO phonons are enhanced with respect to the LO phonons, especially in the sidewall regions, where light enters the sample nearly parallel to the layer, thus activating TO and interface phonons.

- The spectra show differences in different polarization geometries, however, the interpretation is more complicated, as polarizations are mixed due to oblique incidence.

- **Next step:**

experiments with different wavelengths – varying the laser excitation depth in order to see which phonon features are more affected by deeper penetration

Figure 5.17 Raman micro-spectroscopy on FPA arrays with oblique configuration

ACTOPROBE LLC

801 University S.E., Suite 100, Albuquerque, New Mexico, 87106

Phone: +1 (505) 272-7176; Email: aukhanov@actoprobe.com;

www.actoprobe.com

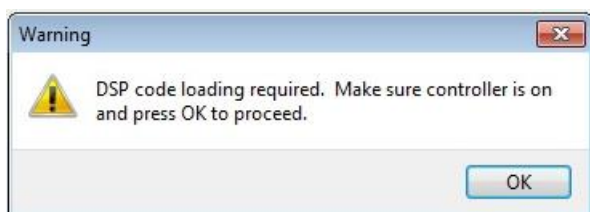
6 Operating Procedures of Actoprobe's TERS system

Start AFM

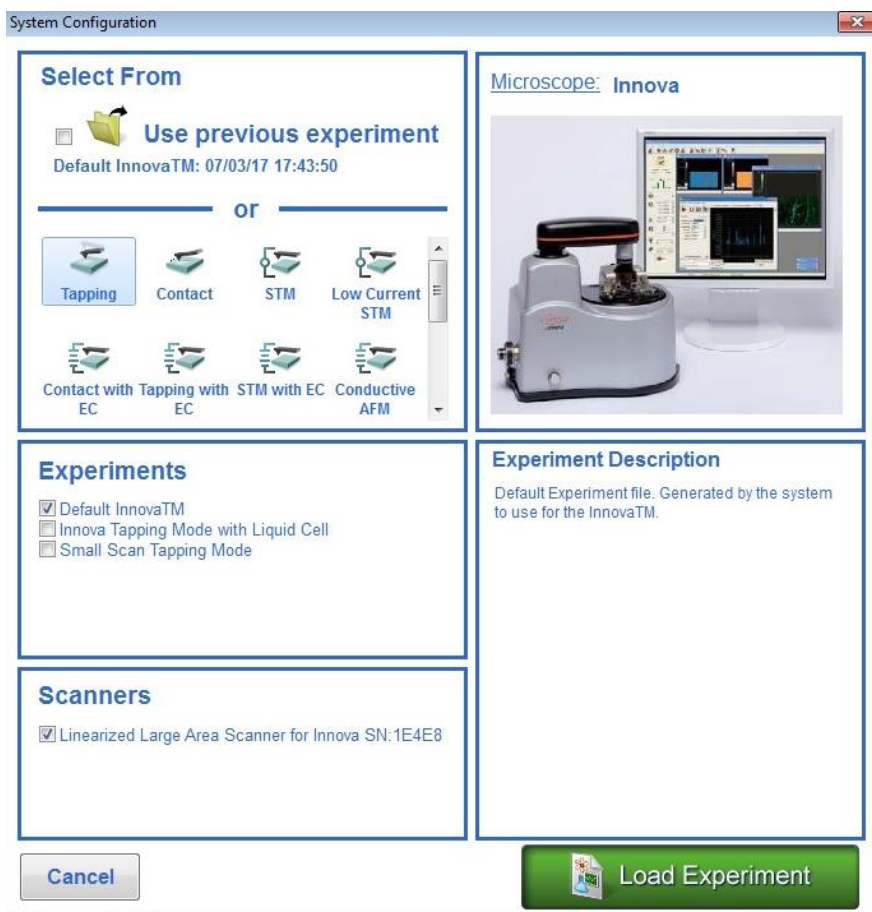
1. Turn on Bruker controller.



2. Open **Nanodrive** software using the icon on the desktop, click **OK**.



3. Select experiment mode, then click **Load Experiment**.



Change Probe (refer to “Innova Probe Mount & Laser Align Video” for details; if using tuning fork probes, refer to “Tuning Fork TERS Experiment Guide – A (013-479-000)”)

1. Raise objective high enough to clear space.
2. Select **Motor Control** tab on the menu bar. Raise probe tip.
3. Change probes and choose the right insert for different mode
4. Change sample if needed
5. Lower probe tip and objective using motor control

AFM alignment (refer to “Innova Probe Mount & Laser Align Video” for details)

1. Adjust objective to focus on tip
2. Align AFM laser on the cantilever
3. To find the laser spot, lower the probe to close to sample surface, where you can see laser scattering
4. Align laser reflection for maximum detector voltage ($>2V$)

AFM image taking (refer to “004-1005-000 INNOVA USER MANUAL-B” for details)

1. In tapping mode, select **Tuning**, check **Auto Tune**, un-check **use current frequency range**
 - ❖ Single amplitude peak is desired during auto-tune
2. Focus on sample surface, lower tip to see the shadows
3. Left click on **Engage** icon
4. Choose image parameter and select data channels
5. Click on **Start**
 - ❖ If z-direction is out of range ($\pm 4.9\mu m$), click Engage and adjust z position in auto mode (optional). If $> 4.9\mu m$ (on the real-time profile window), raise; if < -4.9 , lower

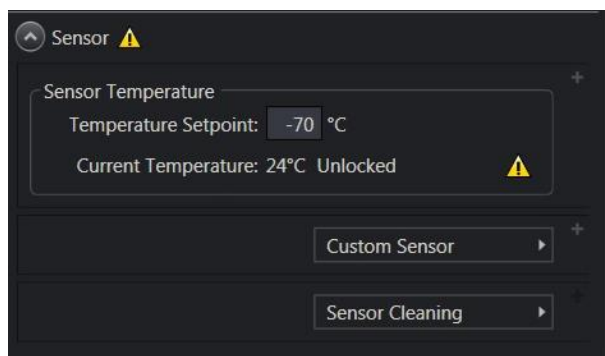
❖ *Do AFM scan before TERS to check integrity of the tip*

Raman spectroscopy (for details refer to “LightField User’s Manual Ver. 4.5”) setup

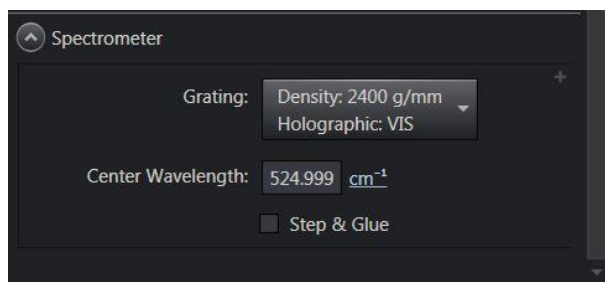
1. Turn on the power supply for spectrometer first, followed by the power supply for CCD
2. Turn on laser controller, use turn-key to turn the laser on



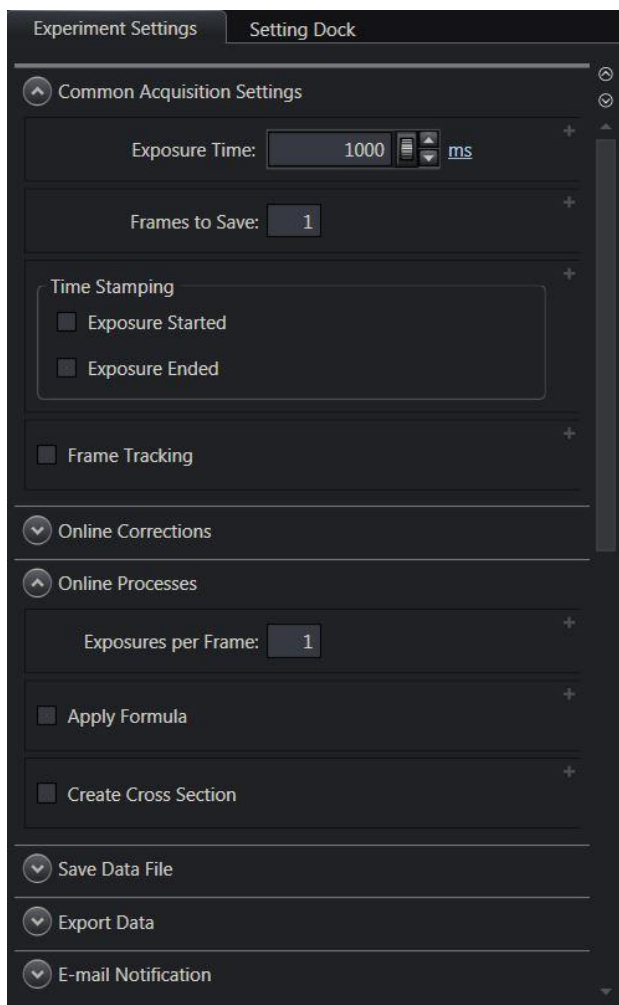
3. Open **Lightfield** software using the icon on the desktop and wait until CCD has reached operating temperature (-70°C)



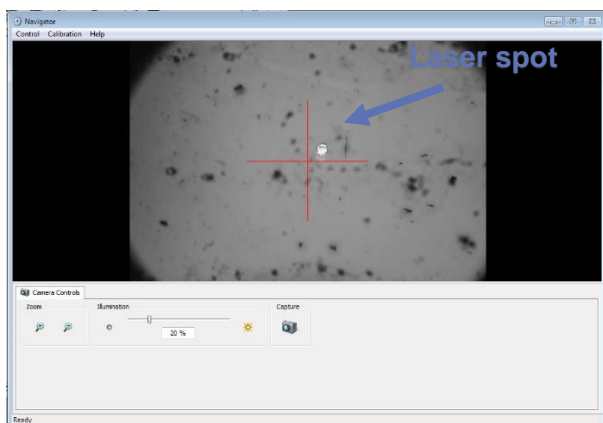
4. Choose desired wavelength from the **Spectrometer** section in the **Experimental Settings** tab



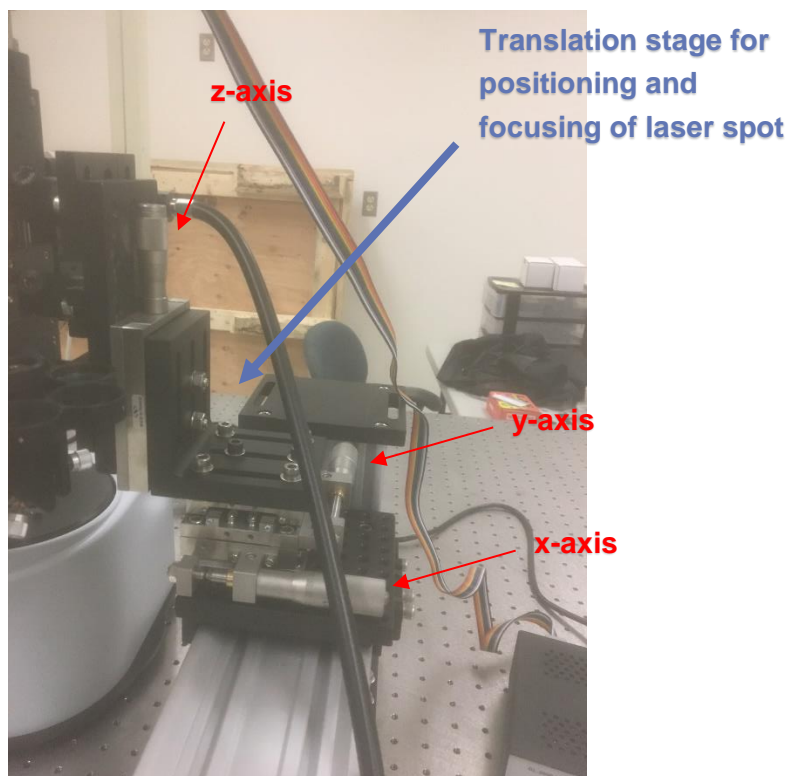
5. Set desired **Exposure Time** in the **Common Acquisition Settings** section and **Exposures per Frame** in the **Online Processes** section



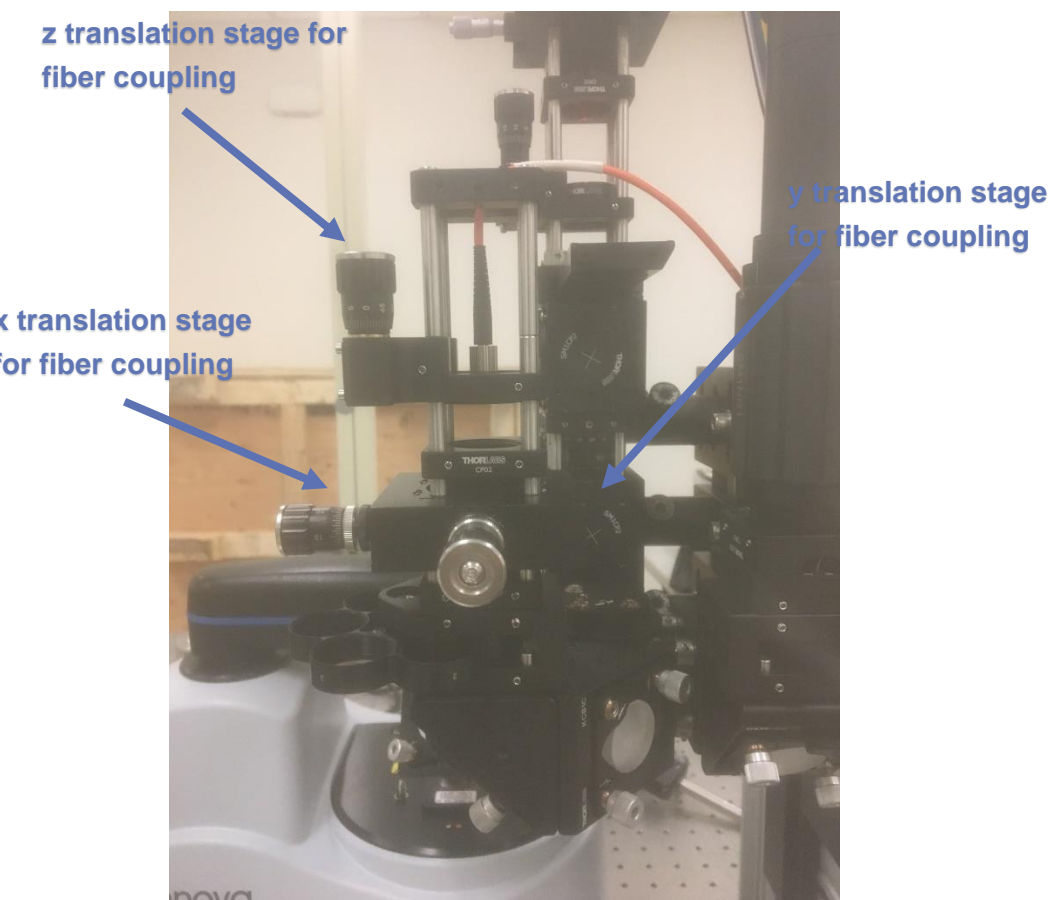
6. Click **Run**
7. Adjust z-axis to achieve minimal spot-size and maximal Raman signal on the sample (Use sliding filters if the camera is overexposed)



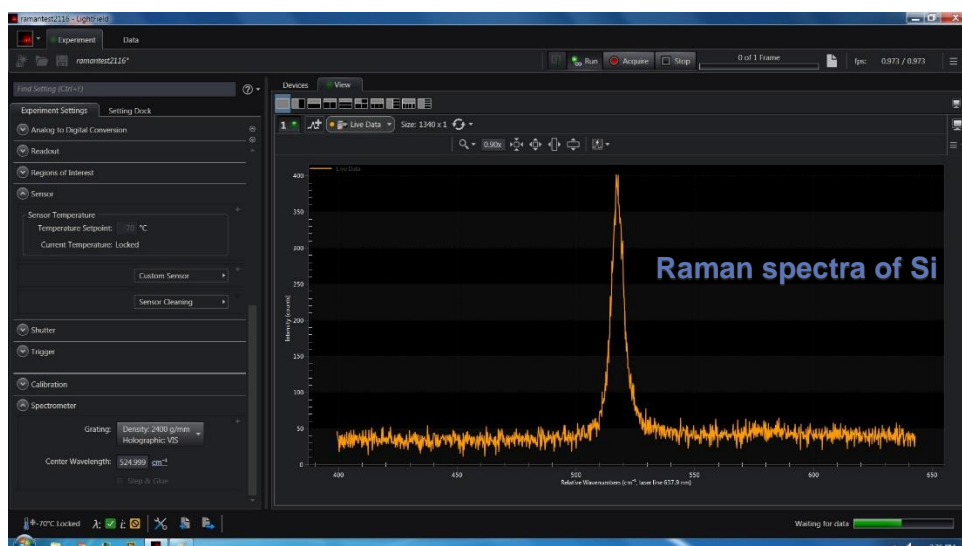
ACTOPROBE LLC
 801 University S.E., Suite 100, Albuquerque, New Mexico, 87106
 Phone: +1 (505) 272-7176; Email: aukhanov@actoprobe.com;
www.actoprobe.com



8. Adjust fiber coupler to maximize Raman signal

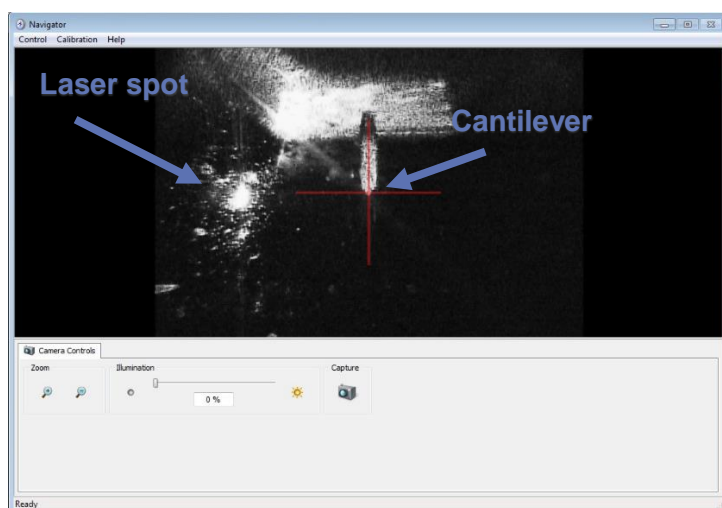


ACTOPROBE LLC
 801 University S.E., Suite 100, Albuquerque, New Mexico, 87106
 Phone: +1 (505) 272-7176; Email: aukhanov@actoprobe.com;
www.actoprobe.com



TERS laser source alignment

1. Align laser to tip and maximize Raman signal using x, y, and z translation stage
 - ❖ It's easier to see the laser spot when the intensity is reduced using the sliding filter
 - ❖ The cantilever and laser spot can also be viewed from the camera
 - ❖ The filtersee the Raman signal



ACTOPROBE LLC
 801 University S.E., Suite 100, Albuquerque, New Mexico, 87106
 Phone: +1 (505) 272-7176; Email: aukhanov@actoprobe.com;
www.actoprobe.com

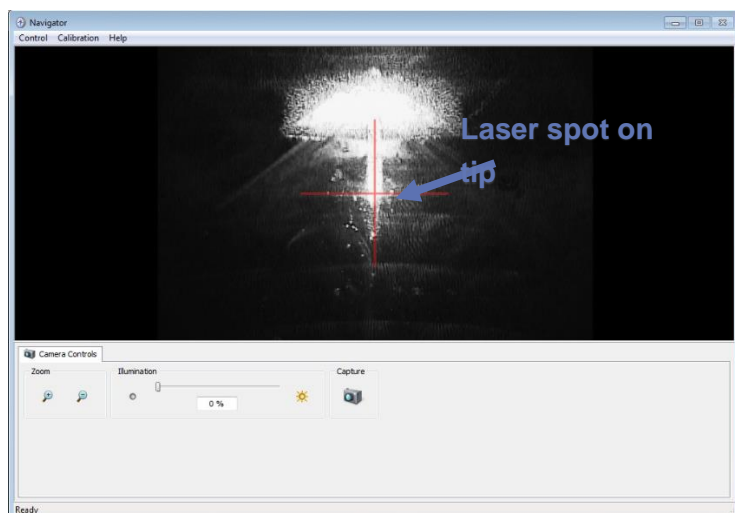


Image through excitation/collection objective with illumination and reduced laser power

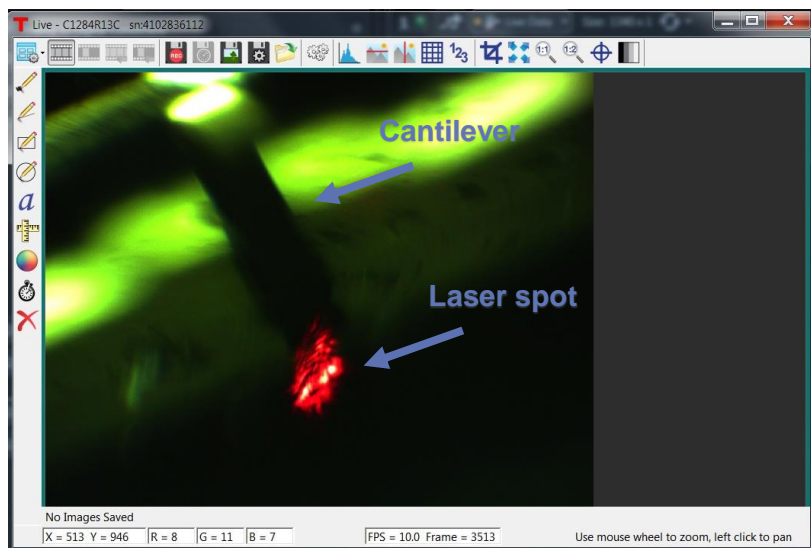
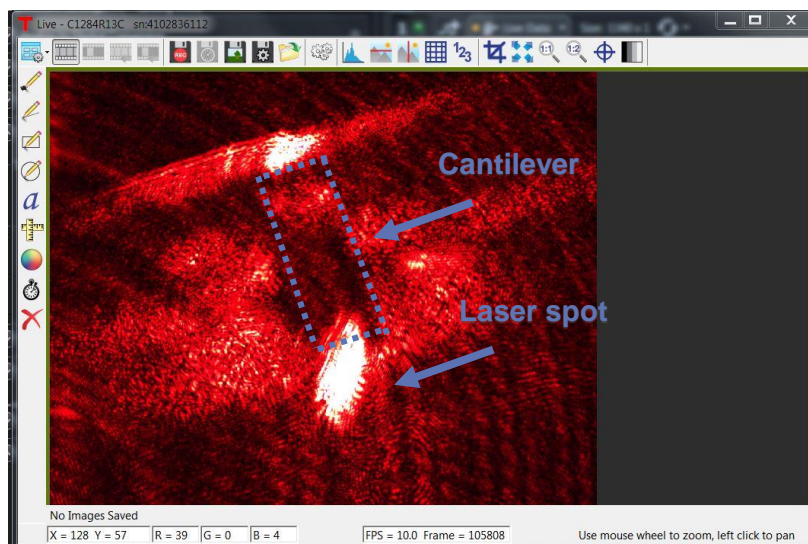


Image through excitation/collection objective without illumination and full laser power



2. Choose parameters for data acquisition
3. Click on **Acquire**

Turn off system

Turn off laser

Dis-engage

Raise probe

Save data

Close Nanodrive software

ACTOPROBE LLC
801 University S.E., Suite 100, Albuquerque, New Mexico, 87106
Phone: +1 (505) 272-7176; Email: aukhanov@actoprobe.com;
www.actoprobe.com

7 Conclusion

In conclusion, Actoprobe team had developed and delivered custom Tip Enhancement Raman Spectroscopy System (TERS) with specially developed Ultra High Aspect Ratio probes for AFM and TERS measurements for small pixel infrared FPA sidewall characterization. This system was tested on real FPA structures and showed very promising results such as TERS on SLS FPA sidewalls, Apertureless NSOM images and AFM morphology for sidewall as deep as 10 μ m.

Interesting results on FPA sidewall were obtained suggesting possibility of achieving stimulated TERS which is very attractive for high resolution chemical analysis.

The delivered instrument should be considered as a minimum feature prototype of a future commercial system for high volume infrared FPA characterization. The future system will be fully automatized and computer controlled. It will include several lasers from UV to Infrared to collect Raman spectroscopy data in broad spectral range for precise chemical analysis. The instrument will be supplied with ultra-fast scanning confocal system to find the most optimal conditions for TERS and many other important features and upgrades.